NTNU – Trondheim
Norwegian University of
Science and Technology

Secondary Hardening in Two Supermartensitic Stainless Steels

Astri Sømme

Materials Science and Engineering
Submission date: June 2012
Supervisor: Jan Ketil Solberg, IMTE
Co-supervisor: Karl Gunnar Solheim, Statoil

Norwegian University of Science and Technology
Department of Materials Science and Engineering

Abstract

Since the late nineties weldable supermartensitic stainless steels (SMSS) has been used in subsea flowlines, and more than 400 km is installed. Hydrogen related problems in the weld fabrication stage or hydrogen induced stress cracking (HISC) due to hydrogen embrittlement under cathodic protection have been reported and testing to better understand the behavior of these materials is of interest. The present work is focusing on the effect of double heat cycles on carbide precipitation and secondary hardening in two high grade SMSS, one alloyed with Ti and one not (0.007% Ti).

The experimental work included heat treatment of both steels in single and double cycles in both oven and in induction heating weld simulator. All specimens were heated to 1000 °C for 30 min to austenize the material and air cooled before simulating second heat cycles of 1-60 min in the temperature range $500 - 600$ °C.

The microstructures resulting from the heat treatments were characterized by standard metallographic techniques, hardness testing and transmission electron microscopy (TEM). The results from hardness testing show a secondary hardening effect in both steels for all temperatures tested, with a maximum for samples treated at 550 °C. For all samples there was also a significant drop in hardness from the hardness of the single cycle sample to the 1 min tempered double cycle samples. From investigation in TEM it was found that, in the steel alloyed with titanium TiC precipitate during tempering and in the steel not alloyed with titanium $Cr_{23}C_6$ precipitate during tempering at 550 °C. The difference in secondary hardening found is explained by the difference in carbide precipitation mechanism. In the steel alloyed with titanium a higher secondary hardening effect was found. No carbide precipitation was found in the single cycle heat treated state of the steels.

Sammendrag

Siden slutten av 90-tallet har sveisbare supermartensittisk rustfrie stål (SMSS) blitt brukt til havbunnsrørledninger, og mer enn 400 km med rør er blitt installert. Problemer relatert til hydrogen i forbindelse med sveising og hydrogen indusert sprekking (HISC) på grunn av hydrogensprøhet fra katodisk beskyttelse har blitt rapportert. Det er ønskelig å undersøke stålet for å forstå oppførselen til denne type material bedre. I oppgaven undersøkes effekten av dobbel varmesykel og sekundærherding i to høy grads SMSS, et legert med titan og et ikke (0.007% Ti).

Det eksperimentelle arbeidet inkluderte varmebehandling av begge stål i enkle og doble sykler ved hjelp av både ovn og sveisesimulator. Alle prøvene ble holdt ved 1000 °C i 30 min for å austenittisere materialet og ble deretter luftavkjølt før en andre varmesykel ble gjennomført i 1-60 min i temperatur området $500 - 600\,^{\circ}\mathrm{C}$.

Mikrostrukturen i prøvene etter varmebehandling ble karakterisert ved hjelp av standard metallografi tekniker, hardhetstesting og transmisjons elektron mikroskop (TEM). Resultatene fra hardhetstesting viser en sekundærherdings effekt i begge ståltypene for alle temperaturer undersøkt, med et maksimum for prøver behandlet ved 550 °C. Det ble observert et signifikant fall i hardhet for alle prøvene fra hardheten i en sykel varmebehandlet tilstand til dobbel sykel varmebehandlet (1 min) tilstand. Etter undersøkelse med TEM ble det funnet at i stålet legert med titan utfelles titan karbid (TiC) og i stålet som ikke er legert med titan utfelles krom karbid ($Cr_{23}C_6$) under anløpning ved 550 °C. Forskjellen i sekundærherding funnet for de to stålene er forklart med forskjellen i utfelling av karbid. Stålet som er legert med titan oppnår en høyere sekundærherdingseffekt en stålet som ikke er legert med titan. Det var ingen karbid utfelling i stålene etter en sykel varmebehandling.

Contents

List of Tables

1 Introduction

Supermartensitic stainless steel (SMSS) is a group of martensitic steels that is based on 13% Cr steel. The supermartensitic stainless steels possess a combination of high mechanical strength, improved corrosion resistance compared to their ancestors and are about 25% cheaper than duplex stainless steels [3]. This combination of factors makes the supermartensitic stainless steels very attractive in the oil and gas production industry. 13% Cr supermartensitic stainless steel are used in flowlines in the offshore sector for transporting well fluid.

The base material for SMSS flowlines is tempered at typically $620 - 650\,^{\circ}\mathrm{C}$ and precipitation of primarily $M_{23}C_6$ carbides intragranulary and on prevoius austenite grain boundaries. This leads to a lowering of hardness and yield stress. Precipitation of carbides also occurs in welding of SMSS, especially for multipass welding where the second weld pass tempers the first. After welding it is in some cases specified a post weld heat treatment (PWHT), typically at $625\,^{\circ}\mathrm{C}$ for 5 minutes, the temperature varies from the outside of the pipe and through the pipe wall, with normally lower temperatures on the inside of the pipe. It is very important that the temperature does not get low enough for secondary hardening to occur instead of tempering and softening of the fresh martensite by precipitation of $M_{23}C_6$ as is the purpose of PWHT.

The precipitation mechanism and precipitation types in the tempering temperature range $500 - 600\,^{\circ}\mathrm{C}$ is of interest to explore as this is a temperature range often used. To better understand the precipitation mechanisms longer tempering times than what is usual for welding is applied in this experimental work. Longer tempering times give larger precipitates, making it easier to investigate.

Precipitates are also found to have an effect on the hydrogen trapping properties of the material [7, 13]. There is a correlation between the precipitate content and the hydrogen in the rest of the material. Hydrogen cracking is one of the main problems experienced with SMSS in pipelines and trapping of hydrogen in retained austenite, dislocations and possibly carbides are important in order to avoid cracking, as the martensite phase is more exposed to hydrogen cracking.

The aim of the present work is to investigate secondary hardening in two supermartensitic stainless steels, one alloyed with titanium and one not (0.007% Ti). This is done by single cycle and double cycle heat treatment to simulate multipass welding of samples of the two steels. Heat treated samples are hardness tested and transmission electron microscopy is used to identify type and distribution of the precipitates

General outline

Section 2 - Theoretical background: In this chapter a theoretical foundation for the material used and precipitates in SMSS will be established. Elementary materials science will not be reviewed.

Section 3 - Experimental: This chapter contains characterizations of equipment and methods used throughout the experimental stage of this thesis. Text and tables are combined with illustrative figures.

Section 4 - Results: In this chapter, results from the experiments will be presented. Seeing as the performed experiments may be divided into different categories, one section will be devoted to each category for each steel type.

Section 5 - Discussion: In this chapter, the results will be analyzed and precipitation mechanisms and types of precipitates will be proposed.

Section 6 - Conclusions: The most important conclusions which could be made from the analysis will in short terms be presented in this chapter.

Section 7 - Further Work In this chapter, the author will propose what should be further researched within the topic. This is based on observations made during experiments as well as personal opinion.

2 Theoretical Background

2.1 Supermartensitic stainless steel

Martensitic 13%Cr steels have been in use for a long time, but without heat treatment these steels show high hardness and low weldability. In the 1990's modifications were done to the martensitic steels in order to improve the weldability and to reduce the hardness. The carbon content was reduced below 0,015wt% and nickel and molybdenum was added. These modifications led to the introduction of the supermartensitic stainless steels [3].

Supermartensitic stainless steels are alloys based on iron and chromium and additions of alloying elements such as nickel, molybdenum and titanium. These steels have a martensitic microstructure at room temperature. In order to improve the properties of SMSS alloying elements are added. Different elements have different effects on the properties of the material. The SMSS are divided in three groups i.e. lean (11Cr-2Ni), medium (12Cr-4.5Ni-1.5Mo) and high (12Cr-6Ni-2.5Mo) alloy grades [12]. Retained austenite is an important part of the microstructure in all of these groups contributing to the mechanical properties of the steels.

The main limitation of SMSS in the offshore sector is hydrogen induced stress cracking caused by H_2S transported as a component in the fluid transported in the flowlines or hydrogen development on the surface from cathodic shield. Fractures have been observed at the anode attachment and the direct cause is a combination of hydrogen content, a sensitive martensitic material and high local stress [19]. It has been found that precipitates can have a hydrogen trapping effect [7, 13] and thus may limit the risk of hydrogen cracking.

In SMSS precipitation of carbides in the material during tempering, multipass welding and during post weld heat treatment (PWHT) has been experienced. These precipitates can have a secondary hardening effect on the material.

In Fig. 1 a section of the ternary phasediagram Fe-Cr-C is shown. Some precipitates are indicated.

2.1.1 Effect of alloying elements

Chromium and nickel
The corrosion resistance of stainless steels is due to a chromium content of minimum 10.5 wt%. Chromium generate a thin, continuous oxide film on the surface of the alloy [3]. Chromium is a ferrite stabilizer which has the property of protecting itself with a passive oxide film and to contribute this property to other metals with which it is alloyed.

The excerpt of the Fe-Cr phase diagram in Fig. 2 shows that an austenitic structure is obtained for chromium content below 12 wt% for a Fe-Cr alloy. A chromium content of 12-14 wt% results in a two-phase area of austenite (γ) and ferrite (δ) and a chromium content greater than 14 wt% gives a completely ferritic structure.

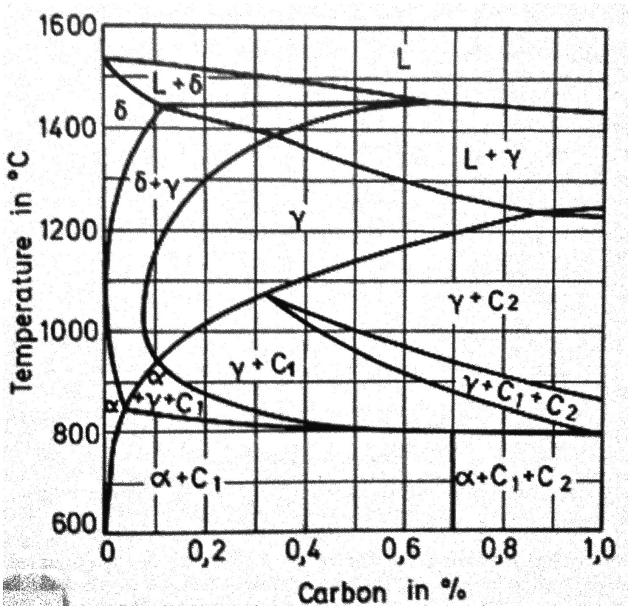

Figure 1: *Section of the ternary phase diagram Fe-Cr-C. Ranges for different precipitates is indicated, C1 is $Cr_{23}C_6$ [13]*

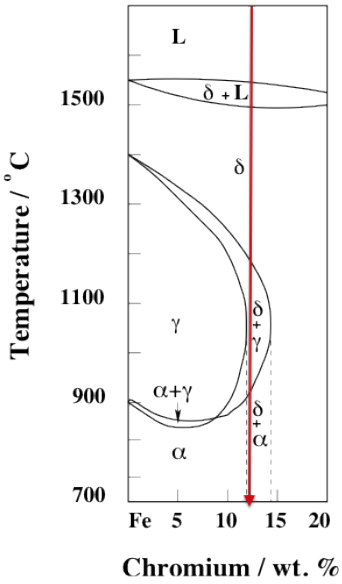

Figure 2: *Range of liquid austenite and ferrite phase in the iron-chromium constitution diagram with a carbon content below 0.01 wt% . The red arrow represents a typical composition of SMSS. [3]*

Chromium constricts the γ region with increasing alloying contents until it disappears completely at around 12% of chromium. This leads to no γ - α transformation above 12% chromium. Chromium strongly promotes the ferrite formation, so that only the δ-ferrite crystallises from the melt over the full alloying range [4].

As the carbon and nitrogen content must be kept low, nickel is added to stabilize the austenite. Nickel is substitutionally solved and can improve the toughness of the material. Nickel expands the austenite (γ-iron) region and therefore acts opposite

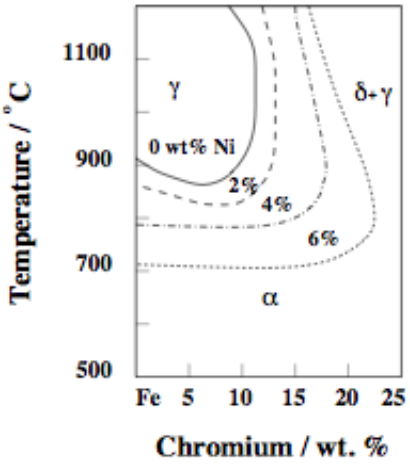

Figure 3: *Influence of nickel on the range of the austenite phase field in the iron-chromium system [3]*

of chromium (Fig. 3). With an increasing content of carbon up to only 0.05% the two-phase area (δ - γ) in Fig. 2 is shifted towards higher chromium contents with the possibility of carbide formation [4]. With an increasing nickel content the austenite region is expanded towards higher chromium contents and lower temperatures. For supermartensitic stainless steels the austenite region is enlarged by addition of nickel to an extent where the formation of δ ferrite, which is an undesirable structural constituent, can be avoided.

Carbon and nitrogen
It is necessary to expand the austenitic field to maintain completely martensitic structure in the presence of molybdenum [3], therefore carbon and nitrogen are added. It is wanted to keep the content of these elements low in order to maintain properties such as weldability.

Even at as low carbon content as 0.02% the formation of carbides in this type of steel is possible. Due to chromiums high affinity to carbon carbides such as $Cr_{23}C_6$, Cr_7C_3 and Cr_3C_2 can be formed [4]. The carbon content in SMSS is very low and therefore carbides of M_7C_3 are usually not formed, but a mixed carbide $(Fe,Cr)_{23}C_6$ (usually indicated as M_{23}) precipitates during post weld heat treatment (PWHT). Nickel does not form carbides. Carbide precipitation in supermartensitic stainless steels is discussed in detail in section 2.1.3.

Molybdenum
To increase the corrosion resistance for transportation of oil and gas, the addition of molybdenum is essential [3]. Molybdenum is a strong ferrite stabilizing element and is balanced by addition of austenite stabilizing elements such as carbon, nitrogen or nickel. The amount of molybdenum added ranges between 0-3 wt% depending on the environment the material is going to be used in. 3% molybdenum qualifies the steel for sour service.

The γ region boundary is shifted to higher temperatures as an effect of addition of

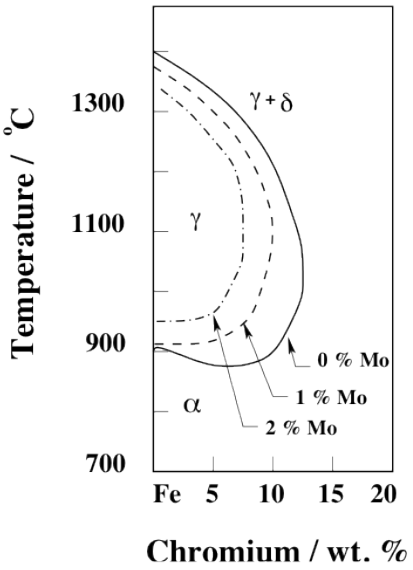

Figure 4: *Effect of molybdenum on the austenite phase stability field in the Fe-Cr phase diagram. Notice how the addition of molybdenum shrinks the austenite field.* [3]

molybdenum, as shown in Fig.4. This is important for PWHT as molybdenum and chromium containing stainless steels must be treated at higher temperatures in order to achieve the α - γ transformation. Molybdenum reduces the solubility of carbon in steel and therefore influence the precipitation of carbides. Carbide precipitation in molybdenum alloyed stainless steels is shifted to higher temperatures, e.g. in austenitic steels to temperatures higher than 700 °C [4]. This effect is only noticeable for martensitic stainless steels with carbon contents below 0.03%, as for SMSS.

Manganese

Manganes is, like nickel, an austenite former and expands the γ region (Fig.3). With increasing manganese contents to 40% the γ -α transformation is shifted to lower temperatures and the austenite becomes stable down to room temperature. SMSS never contain such amounts of manganese and therefore manganese is not the main element responsible for stabilizing the austenite at ambient temperatures [4]. Manganese forms carbides of type $(Fe\text{-}Mn)_3C$, but these are not of importance for stainless steels as carbon is always associated with stronger carbide building elements such as titanium and chromium.

Titanium

Titanium has a strong affinity to carbon and precipitates in the form of stable titanium carbides (TiC). Stainless steels containing titanium are called "titanium stabilized". Titanium carbides is likely to be found in the heat affected zone (HAZ) of a weld if the base material titanium alloyed stainless steel. Titanium constricts the γ region, but this effect only appears if titanium is present in excess, and it is cancelled when titanium is precipitated as stable TiC, TiN or Ti(CN) [6].

2.1.2 Phases in SMSS

SMSS has mainly a martensitic microstructure, but it often contains some retained austenite.

Martensite is formed during cooling of austenite when the cooling rate is too high for diffusion of carbon atoms to occur. The transformation starts when austenite reach the temperature for starting martensite formation, M_s. Normally, to obtain martensitic transformation the steels needs to be rapidly cooled, so that the metastable austenite reaches M_s. The rate of cooling must be sufficient to suppress the higher temperature diffusion controlled ferrite and pearlite reactions, as well as bainite formation [4]. The critical cooling rate is very sensitive to the alloying elements and in general the higher the total concentration of alloying elements, the lower is the critical cooling rate. In the martensite crystal structure carbon atoms are solved interstitially which leads to a contraction of the structure which becomes body- centered tetragonal (bct). The carbon atoms prevents dislocation movement and thus martensite is harder than austenite, and the hardness increases with the carbon content.

Martensite can also form by transformation of austenite when the material is subject to plastic deformation [1].

In alloys with less than 0.6wt% C the martensite will have a needle shape, where the needles are parallel and gathered in larger groups in the structure, called blocks or packages. Fig. 5 is an illustration of the microstructural features of lath martensite. In steels with low carbon content and highly alloyed steels where the M_s temperature is above 200 °C (as it is for SMSS) lath martensite is formed. Martensitic laths are often parallel and form packages (Fig. 5).

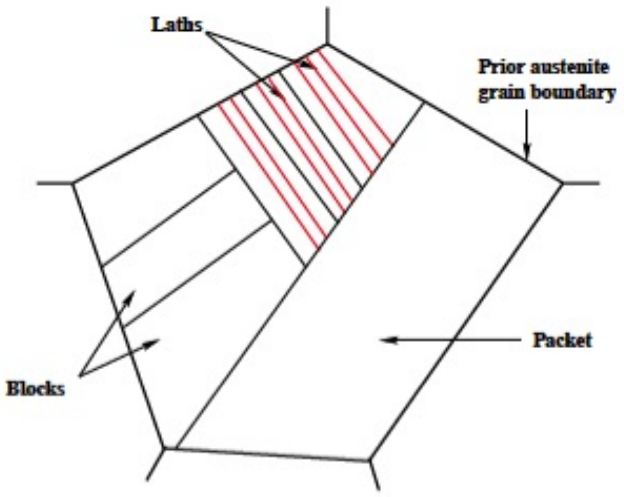

Figure 5: *Schematic illustration of the microstructural features of lath martensite* [3]

Martensite is harder than austenite due to the carbon trapped in the structure. The carbon makes dislocation motion difficult and increases the hardness. SMSS is quite soft due to the low carbon content.

In supermartensitic stainless steels the martensite finish temperature (M_f) is usually in the range of $50 - 150\,^{\circ}C$ so that the M_f temperature is always reached for these steels. It is thus possible to achieve a 100% martensitic structure in these steels [8, 14].

In addition to martensite, retained austenite can be present in the structure. The retained austenite can be present as a result of two processes, incomplete martensitic transformation or as a result of an inter critical annealing.

2.1.3 Precipitation in supermartensitic stainless steel

General
The formation of carbide precipitates is a function of time and temperature, and for SMSS the fastest carbide precipitation takes place around $650\,^{\circ}C$ [4]. The precipitation rate of carbides is very slow in the austenite phase due to increased solubility and decreased diffusion rate of the elements compared to that in ferrite an martensite. During cooling very little precipitation takes place due to that the steel remains austenitic down to a low temperature, thus self tempering in SMSS is not likely to occur and precipitation is only achieved by heating the material after the martensite transformation [13].

Due to their low carbon contents martensitic stainless steels show a lesser tendency towards carbide precipitation than do ferritic 12-17% Cr steels, because at higher temperatures carbon is completely dissolved in the austenitic matrix. This state is still preserved during transformation from austenite to martensite by way of a forced solution. Carbides only precipitate during tempering, partially in the form of coarse carbides at the grain boundaries, but mainly in the grain centers as fine $M_{23}C_6$, together with carbonitrides, producing in most cases a chromium depletion [6].

Due to chromiums high affinity to carbon and the very low solubility of carbon in chromium stainless steels at ambient temperature there is a strong tendency for carbide formation. Carbide precipitation is determined by the diffusion of carbon in the lower temperature range and the increasing carbon solubility in the base material in the higher temperature range and is therefore a time - temperature dependent process.

As was mentioned in section 2.1.1 the excess carbon precipitates as $Cr_{23}C_6$ and seldom as Cr_7C_3 and Cr_3C_2 chromium - iron carbides. $Cr_{23}C_6$-carbides in supermartensitic stainless steels predominantly forms on former austenite grain boundaries which leads to a chromium depletion on the grain boundaries [10]. This makes the material more susceptible to corrosion as the chromium content on the grain boundaries may drop below the resistance limit of approximately 11.5% [4].

Investigations on precipitation formation show that $M_{23}C_6$ is likely to precipitate during PWHT at temperatures higher than $550\,^{\circ}C$ [4]. P.T. Lovejoy [17] studied the effect of PWHT and found that softening of the material occur due to carbide precipitation, maximum softening is achieved for temperatures above $550\,^{\circ}C$ due to precipitation of $M_{23}C_6$. It has been suggested that the $M_{23}C_6$ carbides start to coarsen at higher temperatures and simultaneously new ones appear [4]. This leads

to that carbon continues to be taken out of solid solution and are no longer finely enough dispersed to harden the alloy.

If the martensitic stainless steel is alloyed with titanium, the precipitation of chromium carbides is prevented due to the precipitation of titanium carbides, as mentioned in section 2.1.1. Titanium has higher affinity to carbon than chromium and thus stable titanium carbides of the MC type precipitate [16]. This type of carbide require much more carbon than $M_{23}C_6$, and therefore if the amount of titanium in the steel is sufficient all the carbon can be involved in precipitation of titanium carbides and preventing the precipitation of chromium carbides. This leads to all the chromium staying in solid solution and thus no chromium depletion in the areas around the precipitates and the corrosion properties are kept.

In addition of the precipitation of carbides in martensitic stainless steels, nitrides and intermetallic phases may also precipitate. M_2X, MX nitrides may reduce the corrosion resistance and cause secondary hardening during tempering [15].

An effect of precipitation in SMSS is secondary hardening. The carbides that precipitate during tempering between 400 °C - 600 °C can give a hardening effect, resulting in a smaller hardness drop after tempering.

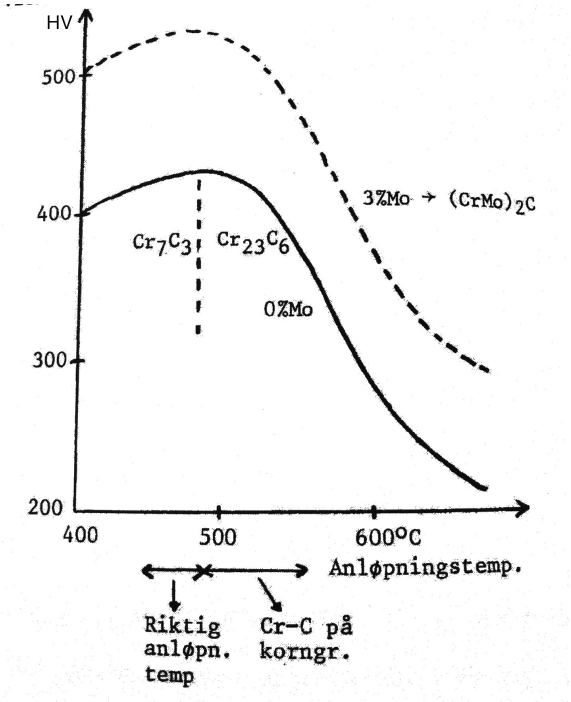

Figure 6: *Secondary hardening in a supermartensitic stainless steel. [10]*

The supermartensitic stainless steels have an austenite area as their M_s temperature is above room temperature and are therefore hardenable. The high chromium content gives good hardenability and air cooling is sufficient to obtain hardening.

Subsequent tempering gives a secondary hardening effect. Tempering at temperatures 400 °C to 475 °C gives Cr_7C_3-carbides and thus a secondary hardening. But,

the corrosion resistance of the steel will be lowered as the carbide precipitates lower the amount of chromium in the matrix.

For steels with low carbon content secondary hardening leads to a lowering of the toughness of the material.

At higher tempering temperatures the Cr_7C_3 carbides transforms to $Cr_{23}C_6$ and the alloy overage. At higher tempering temperatures, ex. 600 °C, the chromium depletion at the grain boundaries will even out due to diffusion, and therefore does not affect the steels resistance to corrosion.

The secondary hardening effect can be increased by addition of molybdenum as can be seen in Fig. 6. This effect is due to the precipitation of $(Cr,Mo)_2C$

Change in the size and shape of the TiC precipitated with tempering temperature is suggested to be like indicated in Fig. 7 by Wei and Tsuzaki [5]. For tempering temperatures 500 °C - 600 °C the precipitates are likely to be flat disks with increasing diameter and thickness with increasing temperature. Tempering in this temperature regime is in the α-phase.

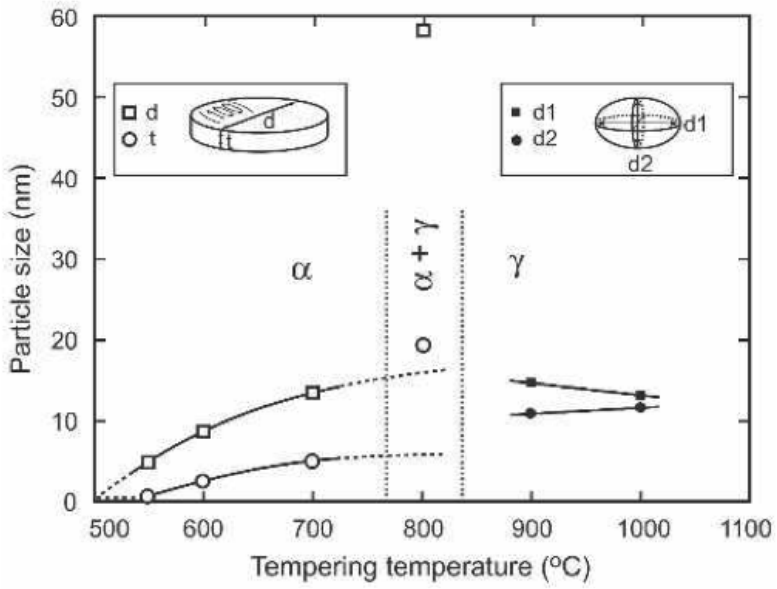

Figure 7: *Change in the size and shape of the TiC precipitate with tempering temperature. The matrix phases are indicated [5]*

Precipitation during multipass welding

During multipass welding the first weld pass will be tempered by the second weld pass, and thus carbides will precipitate. Fig. 9 is a schematic illustration of tempering of first weld pass from second weld pass. During the first weld pass the base metal is heated up to the austenitic phase and remains austenitic until the martensite transformation starts at the M_s-temperature. The solubility of carbon in austenite at room temperature is 0.006%, and it remains very low up to 800 °C [6]. The excess carbon precipitates mainly as $M_{23}C_6$ chromium-iron carbides. Fig. 8 is a schematic illustration of second heat cycle in heat affected zone by subsequent weld

pass, which is of importance for this present work.

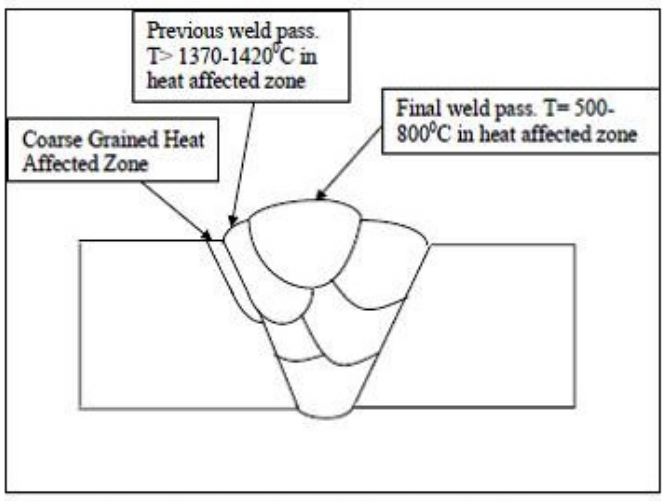

Figure 8: *Schematic illustration of second heat cycle in heat affected zone by subsequent weld pass [13]*

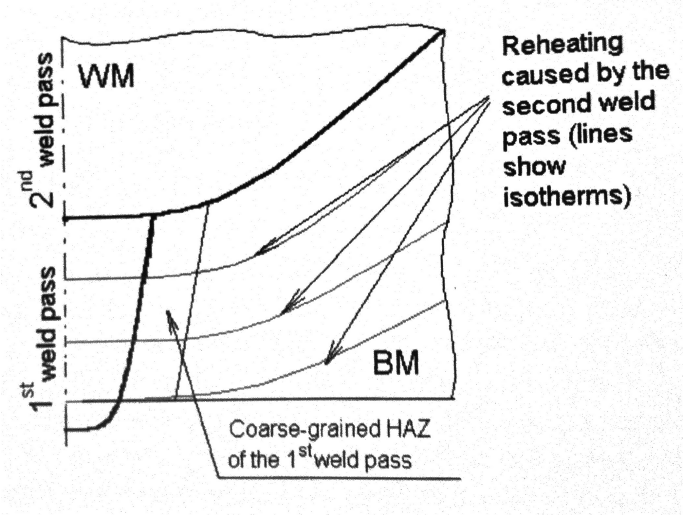

Figure 9: *Schematic illustration of tempering of first weld pass from second weld pass: WM - weld metal; BM - base metal [16]*

2.2 Hydrogen trapping

One of the main problems with SMSS experienced in the North Sea is hydrogen induced stress cracking due to hydrogen in the material. Hydrogen in pipelines where well fluid is flowing experience hydrogen from the well fluid and some hydrogen development on the surface du to the cathodic shield.

There are known hydrogen trapping sites in SMSS, ex. dislocations and retained austenite but it is also suggested that precipitates can act as hydrogen traps. Rosenquist [7] researched the effect of precipitates on hydrogen trapping in his master the-

sis and found that the carbides trap the hydrogen on its sides and the ability to trap hydrogen increases with the incoherent bond to the lattice. Wei and Tsuzaki [5] has also done some research on this phenomenon. The primary purpose of the study was to examine the evolution of the hydrogen-trapping property when the TiC particles changes from a coherent to an incoherent particle.Wei and Tsuzaki [5] found that the amount of hydrogen trapped decreases with increasing tempering temperature above 550 °C, regardless of alloy composition and thermal history.

3 Experimental Method

3.1 Material

Two steels were used for the present study, designated steel A and steel B. Both steels are typical pipeline materials and are considered "rich" grade supermartensitic stainless steels.Their compositions are shown in Tab. 1. Steel A is alloyed with titanium and steel B is not (0.007% Ti). Both steels were received in the form of pieces of pipelines from the North Sea.

Table 1: *Chemical composition in wt% of material used*

	Element							
	C	Si	Mn	P	S	Cr	Ni	Al
Steel A	0.006	0.120	0.440	0.013	0.002	12.000	6.400	0.030
Steel B	-	0.190	0.700	0.006	<0.001	12.400	5.860	0.035
	Element							
	Mo	Nb	V	Ti	Co	B		
Steel A	2.500	<0.010	0.040	0.110	0.040	<0.001		
Steel B	2.210	0.002	0.049	0.007	0.046	-		

Steel A chemical composition is from the material certificate and the chemical composition of steel B is found by optical spectrum analysis at Statoil Rotvoll.

3.2 Heat treatment

Both steels were in first heat cycle austenitized at 1000 °C for 30 minutes and air cooled in order to achieve a microstructure consisting of fresh martensite. Air cooling was sufficient as both steels are self hardening and a martensitic structure is expected. The samples were then as a second heat cycle tempered at different temperatures and different times as shown in Tab. 2.

Two different heating methods were used in this experiment. Narbertherm C290 oven was used for the first heating cycle and the second heating cycle for longer tempering times and Smitweld Thermal Cycle Simulator, model 1405 was used for shorter tempering times. Fig. 10a and Fig. 10b show the Nabertherm C290 oven and the Smitweld Thermal Cycle Simulator respectively.

Before weld simulation the test materials were machined into 10 x 10 x 70 mm specimens. The Smitweld heats a narrow zone 3-5 mm wide in the centre of the sample by resistance heating. The sample is held by water cooled copper clamps that supply the electric current to the sample. By regulation of the current through the sample the heating and cooling rates are controlled. All samples were tested with a thermocouple of type K welded to the middle of the specimens in order to control the temperature during the simulation.

Table 2: *Second heat cycle temperatures (T2) and times (t2) for samples of steel A and steel B. All samples were water cooled after heating*

Second cycle heat treatment steel A and B		
T2 [°C]	t2 [min]	Type
500/ 550/ 600	1	Smitweld
500/ 550/ 600	2	Smitweld
500/ 550/ 600	10	Nabertherm
500/ 550/ 600	11	Nabertherm
500/ 550/ 600	12	Nabertherm
500/ 550/ 600	13	Nabertherm
500/ 550/ 600	14	Nabertherm
500/ 550/ 600	15	Nabertherm
500/ 550/ 600	16	Nabertherm
500/ 550/ 600	17	Nabertherm
500/ 550/ 600	18	Nabertherm
500/ 550/ 600	19	Nabertherm
500/ 550 /600	20	Nabertherm
500/ 550/ 600	30	Nabertherm
500/ 550/ 600	60	Nabertherm

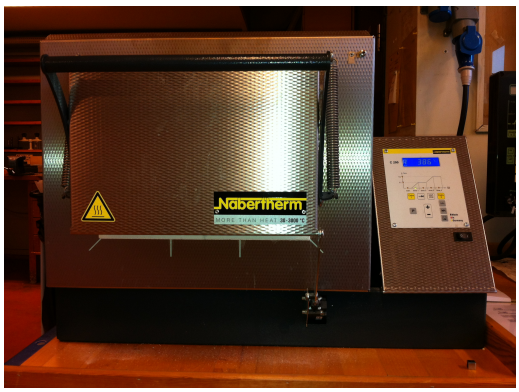

(a) *Nabertherm C290 oven*

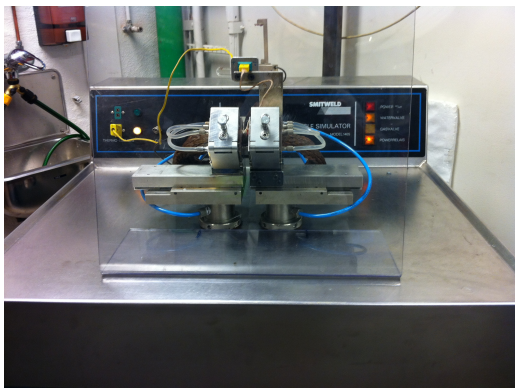

(b) *Smitweld Thermal Cycle Simulator, model 1405*

Figure 10: *Equipment used for heat treatment of samples. The Nabertherm C290 oven in Fig. 10a is used for longer holding times at second heat cycle temperature, T2 and the Smitweld Thermal Cycle Simulator in Fig. 10b is used for shorter holding times at temperature T2*

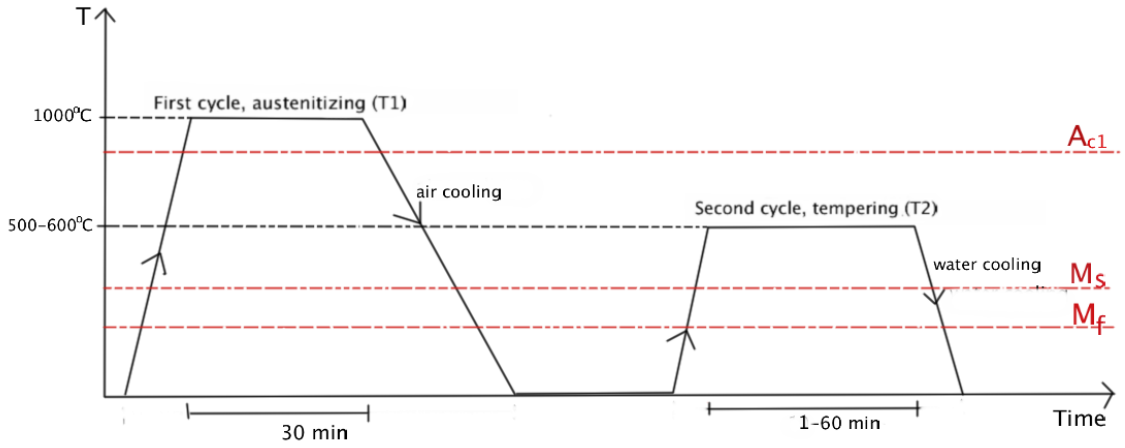

Figure 11: *Illustration of heating cycle for samples of steel A and steel B heated in Nabertherm C290 oven. All samples were austenitized at T1=*1000 °C*/30min and then some samples were tempered at T2=*500 − 600 °C*/1-60min*

Samples to be treated in Nabertherm C290 oven were cut into 10 x 10 x 10 mm specimens. Specimens were treated at different T2 varying from 500 °C to 600 °C and tempering times were varied from 10 to 60 minutes (Fig.11).

Samples to be treated in Smitweld Thermal Cycle simulator were treated at different T2 varying from 500 °C to 600 °C and tempering times varying from 1 to 2 minutes (Fig.11). Note that the time to tempering temperature T2 is much shorter for the Smitweld Thermal Cycle Simulator than for the Nabertherm C290 oven.

3.3 Metallography

All tested specimens were cut in two in the middle and then ground and polished.

3.3.1 Light microscopy

Specimens for light microscopy were etched with 50% Marble's etchant (Marbles etchant consists of 4g $CuSO_4$, 20mL HCl, 20mL H_20) for three seconds in order to reveal the microstructure. The light microscope used was Leica MeF4m with digital camera Jenoptik Laser Optik Systeme camera type ProgRes C10 plus.

3.3.2 Hardness testing

Vickers hardness in the centre of the samples was found for all heat treated specimens, ten readings per specimen. Vickers hardness was tested with Matsuzawa DVK-1S hardness tester with a load of 5kg, loading time of 15 seconds and loading speed 100µm/sec. Vickers hardness is denoted as [HV5].

3.3.3 Preparation of carbon replicas for transmission electron microscopy

Samples of steel A and B tempered at T2=550 °C were chosen for transmission electron microscopy (TEM) investigation as maximum secondary hardening was experienced at this temperature for both steel A and steel B. For TEM investigation carbon replicas of the specimens were prepared.

Table 3: *Preparation of samples for investigation with TEM*

Steel	**T1 [°C]**	**T2 [°C]**	**t2 [min]**
A	1000	-	-
A	1000	550	2
A	1000	550	15
A	1000	550	20
A	1000	550	30
A	1000	550	60
B	1000	-	-
B	1000	550	2
B	1000	550	60

The etch is used to isolate the precipitates from the bulk material on a replica, while still preserving the original phase distribution in the surface section taken from the bulk [2]. This method is well suited for the study of carbide precipitates in steels, where an extraction replica can reveal the composition, crystal structure and morphology of the carbide phases that would otherwise be obscured by the strong diffraction contrast and X-ray excitation of the ferrous alloy matrix.

To prepare carbon replicas the ground and polished samples were etched for 1 minute in an etch consisting of:

14 ml	HF
6 ml	HNO_3
40 ml	H_2O

After etching a carbon film was coated on the sample surface with Agar Turbo carbon coater with a 3 times 8 seconds application time of carbon. The carbon film was cut in 2mm X 2mm squares before the sample was put in a second etch to extract the carbon replicas. The etch consists of:

14 ml	HF
4 ml	HNO_3
60 ml	H_2O

The sample was kept in the etch until all the replicas loosened from the surface. The replicas were picked up from the etchant on 3 mm copper grids and cleaned in ethanol. Fig. 12 is a schematic illustration of the steps in carbon replica preparation.

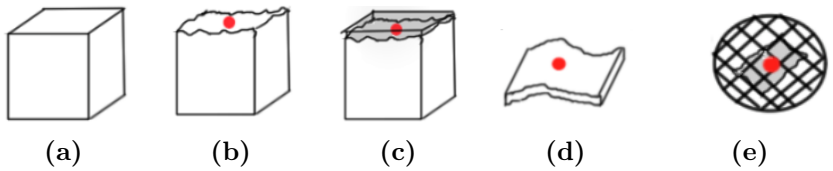

Figure 12: *Illustration of carbon replica sample preparation. (a) Mechanically ground and polished sample (b) Etched surface, red dot indicating precipitate (c) Carbon coating on etched surface (d) Carbon layer with precipitate etched off (e) Carbon replica on copper grid*

3.4 Transmission electron microscopy

The TEM instrument used was a Jeol JEM-2010 microscope with a Gatan CCD camera and equipped with an energy dispersive x-ray detector,EDS of the type EDAX Sensor AMETEK, for chemical analysis. Bright field imaging, electron diffraction imaging and EDS analysis were used in this experiment to characterize the precipitates.

3.4.1 Bright field imaging

Imaging of small particles in metals is an important use of TEM. Bright field imaging was used in this work. This imaging technique dark precipitates on a bright background. This is because in bright field imaging the spread beam from the particle (Fig. 13) will be stopped by the objective aperture and very little light will come through to the image of the particle. In the matrix on the other hand the electrons goes right through the sample and to the image. The particle will therefore be dark on a bright background in bright field imaging [11].

Thus it will be possible to see the precipitates in the carbon matrix.

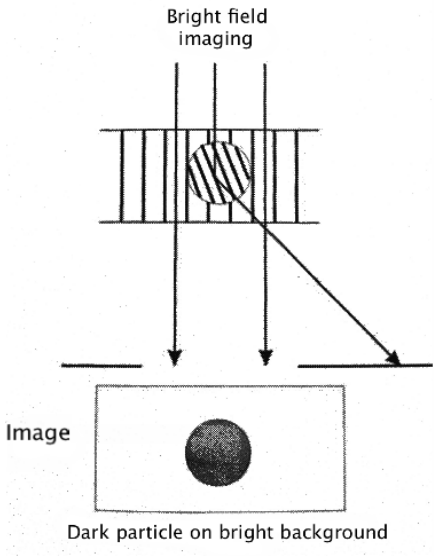

Figure 13: *Bright field imaging in TEM [11]*

3.4.2 Diffraction imaging and indexing of diffraction patterns

Only for some angles of incident are all reflections from the parallel planes added in phase and give a strong reflection. Bragg's law (Eq. 1) does not refer to the arrangement of atoms in each lattice point, but the atom density around the lattice point determines the relative intensity between reflections of different order from a given set of parallel lattice planes.

Those sets of lattice planes that are oriented parallel with the incident beam will give constructive interference. All other planes will give destructive interference. Although Bragg's law (Eq. 1) only can be fulfilled for one order of reflections at the same time, multiple reflection orders from the same lattice plane will appear in the diffraction image.

$$2d_{hkl}sin(\theta) = n\lambda \tag{1}$$

$$Rd = R_{scale}\frac{1}{5}nm \tag{2}$$

where R is the distance between a first order reflection and the central reflection in the photo and R_{scale} is the length of the scale bar in the diffraction image (ex. Fig. 22b) and 1/5 is the scale of the image.

The reflections in an electron diffraction image make a two dimensional periodic lattice pattern. The distance from the central reflection and out to each of the other reflections is reversely proportional with its plane distance. Eq. 3 is the expression for the plane distance, d, for cubic crystals, where (hkl) is the index of the reflection and a is the lattice parameter.

$$\frac{1}{d^2} = \frac{h^2 + k^2 + l^2}{a^2} \tag{3}$$

Independent of which crystal direction the incident beam is coming the diffraction image will have a periodic lattice pattern and the positions of the reflections and the *hkl*-indexes can be found by vector addition. For a cubic crystal the incoming beam must be parallel with one of the crystal axis to give a quadratic pattern.

Fig. 14 shows the distances and angles in an electron diffraction image. In a diffraction image it is common to name the reflections according to the lattice planes it originates from.

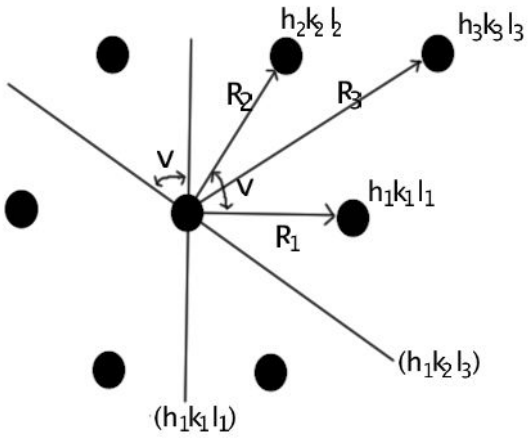

Figure 14: *Distances and angles in a diffraction image*

By finding the ration between the length from the central reflection to a first order reflection of two reflection points (*hkl*) can be found from a table in TEM literature (such a table is found in [10]). Then by using the angle between the two reflections and the indexes found from the length ratio the correct sign of the index can be found by the use of Eq. 4.

$$[h_1k_1l_1] \cdot [h_2k_2l_2] = |[h_1k_1l_1]| \cdot |[h_2k_2l_2]| \cdot \cos v \tag{4}$$

When the indexes for 1 and 2 is found, the sum of $[h_1k_1l_1]+[h_2k_2l_2]$ has to be checked to give the correct indexes for $h_3k_3l_3$. If it does not the indexes for 1 and 2 has to be checked again until they are in compliance.

For some combinations of *hkl* the intensity will be zero and the reflection is extinguished. For face centered cubic crystals (*FCC*) the *hkl* have to be either all odd or all even numbers in order to get a reflection [11].

The TEM samples used in this experiment are carbon replicas. As carbon is an amorphous material it will not give a diffraction pattern, thus diffraction patterns found will originate from a precipitate.

Table 4: *Structural data for some carbides from Pearson's Handbook of Crystallographic Data for Intermetallic Phases citepearson*

Phase	Structure type	Pearson symbol space group	a [nm]
CCr	ClNa	cF8 $Fm\bar{3}m$	0.362
C_6Cr_{23}	C_6Cr_{23}	cF116 $Fm\bar{3}m$	1.0650
C-Cr-Fe	C_6Cr_{23}	cF116 $Fm\bar{3}m$	1.0578
		hP80	1.3815 c=0.4498[a]
C-Ti	ClNa	cF8	0.43176
C-Ti	Mg	hP2	0.2955 c=0.4702[a]
C_2Ti		cP3	0.313

[a] this is a hexagonal structure and thus has a c-axis lattice parameter

4 Results

4.1 Heat treatment

Two different heating methods were used for the samples. Temperature measurements of the two gives a heating cycle as indicated in Fig. 15. Note the difference in time to condition temperature for the two. The Smitweld simulator is set to reach 550 °C after 5 seconds, whilst after testing with samples connected to a K-type thermocouple in the centre it was fount that the Nabertherm C290 oven needs 5 minutes to heat the 10x10x10 mm sample to 550 °C in the centre of the sample.

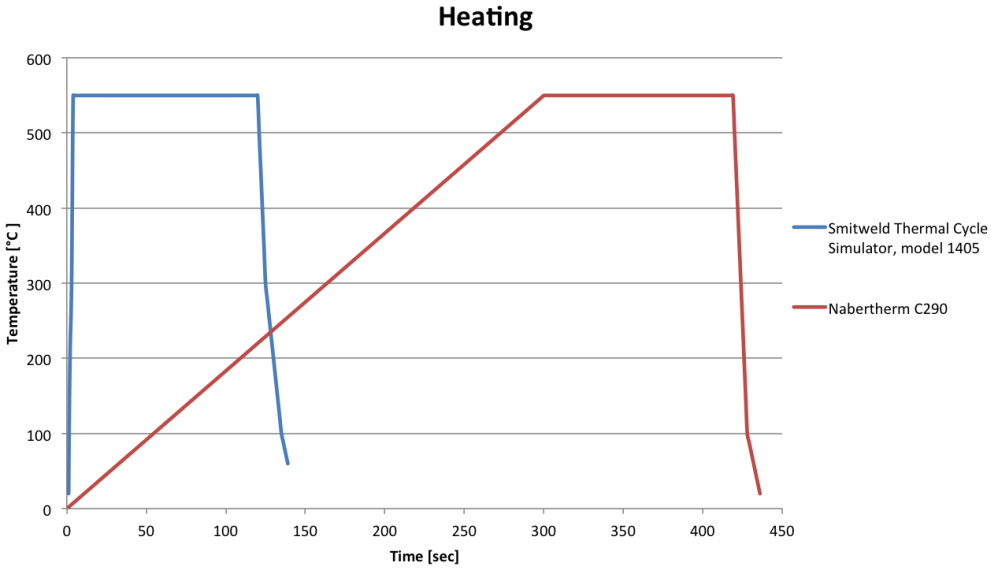

Figure 15: *Time to* 550 °C *for the two heating methods used in this study*

To achieve suffiecient tempering time at the correct temperature, five minutes was added to the time the samples were held in the Nabertherm oven.

4.2 Steel A

4.2.1 Hardness testing

As all samples received different second cycle heat treatments, the austenitized state of the material was characterized before second cycle heat treating. The hardness of the austenitized steel A and all the tempered samples is shown in Tab. 5

All hardness measurement results are tabulated in Appendix as well as the standard deviations.

After tempering steel A at different times and temperatures, the hardness in the centre of the samples was measured. Fig. 16 shows the hardness in the centre of the samples as a function of holding time at 500 °C for steel A.

Table 5: *HV5 value as a function of holding time at temperatures* 500 °C, 550 °C *and* 600 °C *for steel A. Each HV5 value is an average of ten readings (all readings are presented in Appendix)* σ *represents the standard deviation of the readings*

t2	austenitized		T2=500 °C		T2=550 °C		T2=600 °C	
[min]	[HV5]	σ	[HV5]	σ	[HV5]	σ	[HV5]	σ
0	369	5	-		-		-	
1	-		354	5	353	5	340	7
2	-		359	5	360	5	342	7
11	-		368	8	363	4	368	6
12	-		369	6	375	6	361	7
13	-		373	4	372	3	352	6
14	-		374	7	371	5	350	7
15	-		367	7	370	13	350	5
16	-		366	4	369	6	348	5
17	-		365	4	364	6	346	4
18	-		366	3	363	7	341	6
19	-		365	7	361	6	341	5
20	-		364	5	357	3	344	4
30	-		363	3	362	10	339	3
60	-		352	4	360	12	339	5

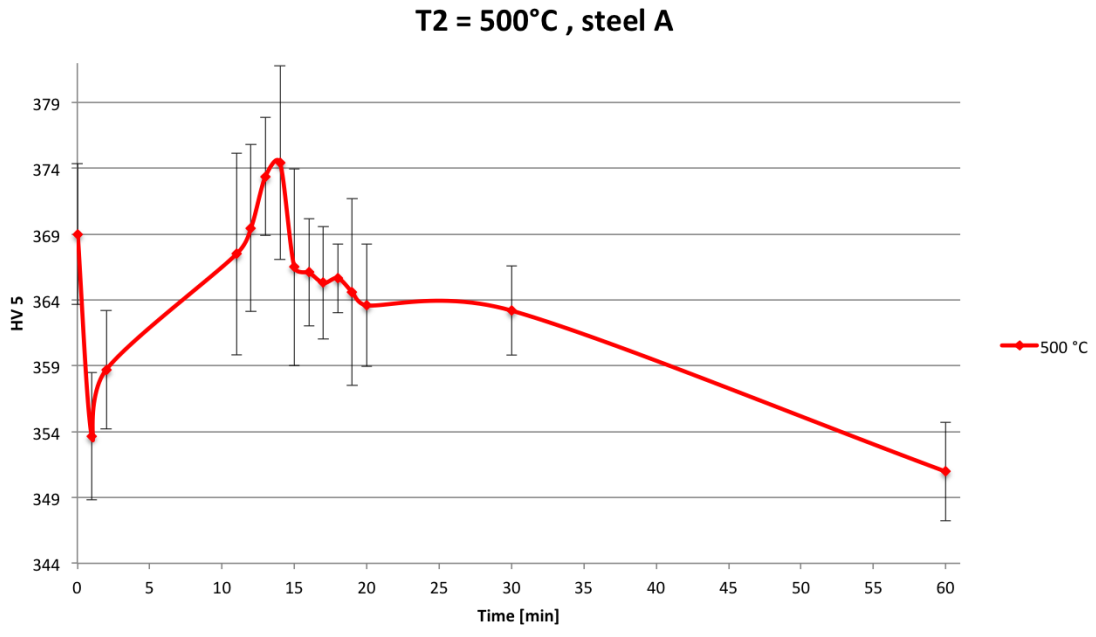

Figure 16: *HV as a function of time at T2*=500 °C *for steel A, average of ten readings.*

Fig. 16 show that there is a decline in hardness from 30 minutes tempering and towards 60 minutes tempering for the sample tempered at 500 °C. Note that the hardness after 60 minutes tempering is lower than that after 1 minute tempering (Fig. 16).

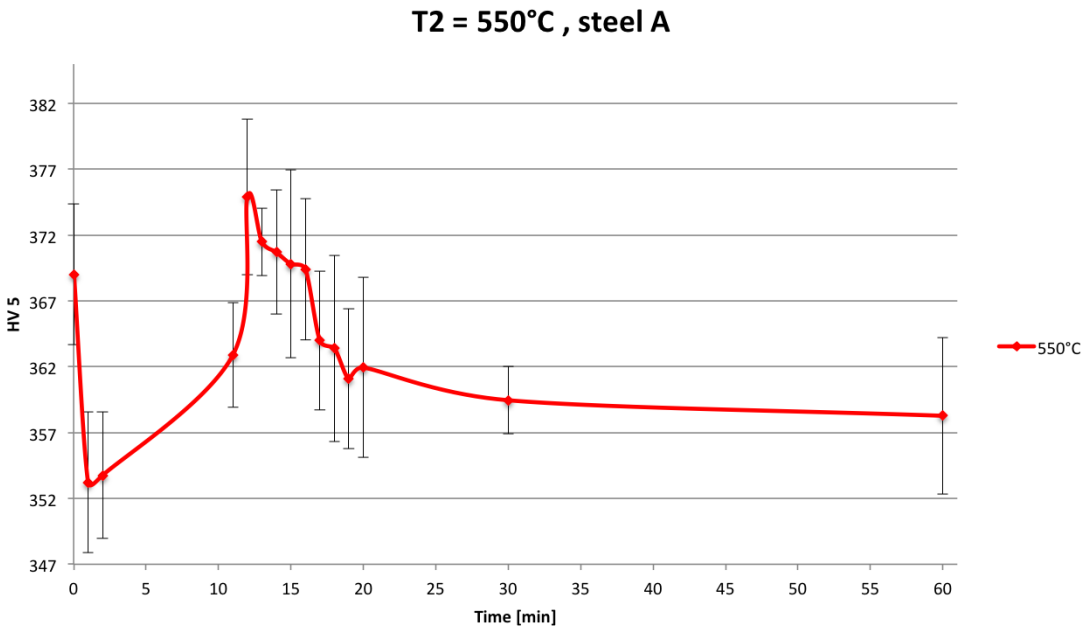

Figure 17: *HV as a function of time at T2*=550 °C *for steel A, average of ten readings.*

Fig. 17 show that the hardness of the sample tempered at 550 °C level off from the 20 minutes tempered sample toward the 60 minutes tempered sample. Note that the hardness of the samples tempered for 30 and 60 minutes is higher than that of the sample tempered for 1 minute (Fig. 17).

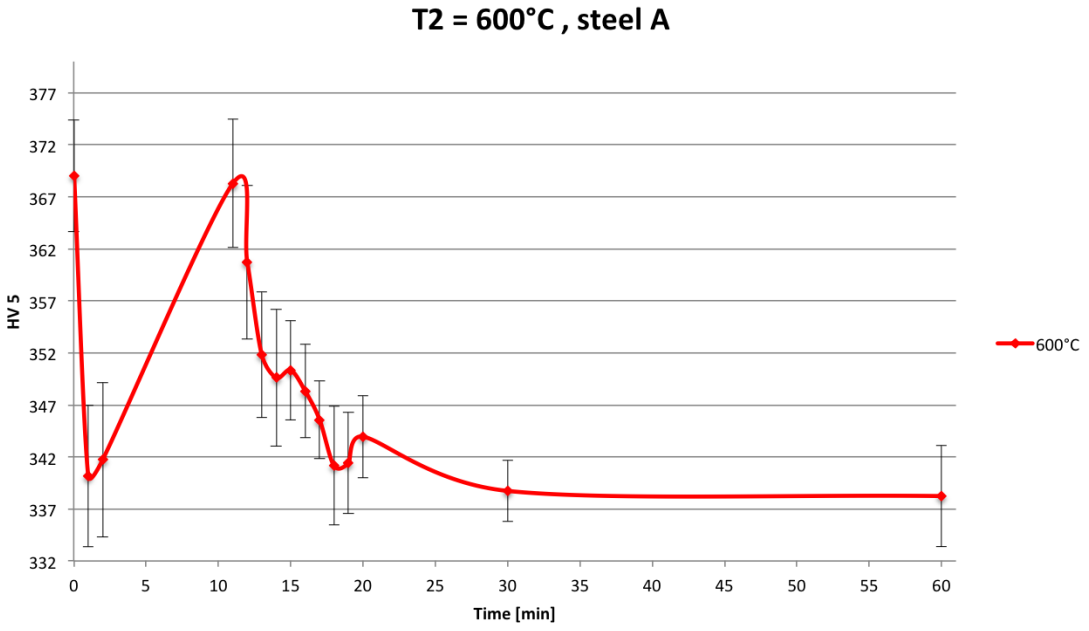

Figure 18: *HV as a function of time at T2*=600 °C *for steel A, average of ten readings.*

Fig. 18 show that the hardness of the sample tempered at 600 °C is quite stable from thirty minutes towards 60 minutes tempering. Note that the hardness after 1

minute tempering and the hardness after 30 and 60 minutes tempering is the same.

Fig. 16, 17 and 18 shows that the highest hardness is achieved for the steel tempered at 550 °C with a maximum hardness of HV5 375 after 12 minutes at 550 °C. The lowest hardness is achieved for the steel tempered at 600 °C for 1 minute with a HV5 340. The steel tempered at 500 °C achieves its hardness maximum after longer tempering time than for the steels tempered at 550 °C and 600 °C. The samples tempered at 600 °C reaches its hardness maximum after 11 minutes of tempering.

Note that for samples tempered at 500 °C and 550 °C the maximum hardness achieved after tempering is higher than that of the austenitized state. The sample tempered at 600 °C does not achieve such a high hardening effect from tempering.

Also note that for all three temperatures explored (500 °C, 550 °C, 600 °C) there is a significant drop in hardness from the austenitized state to the 1 minute tempered state.

Tab. 6 show some key results from the hardness measurements of the samples of steel A tempered at $500 - 600$ °C for different times.

Table 6: *Key results from hardness testing of tempered samples of steel A*

Tempering temp. (T2)	**Max.hardness, tempered state**		**Min.hardness, tempered state**	
	[HV5]	t2 [min]	[HV5]	t2 [min]
500 °C	374	14	352	60
550 °C	375	12	353	1
600 °C	368	11	339	30

4.2.2 Metallographic examination

Light micrographs of steel A after austenitizing at T1=1000 °C/30min and after tempering at T2=550 °C/60min is shown in Fig. 19 (a) and (b) respectively.

Fig. 19a show the austenitized microstructure of steel A. Parallel martensite laths gathered in packages are visible.

Fig. 19b show the microstructure of steel A after two heat cycles, T1=1000 °C/30 min and T2=550 °C/60min. Some darker martensite areas are seen, compared to that of the austenitized microstructure. This is tempered martensite, and the brighter areas can be fresh martensite.

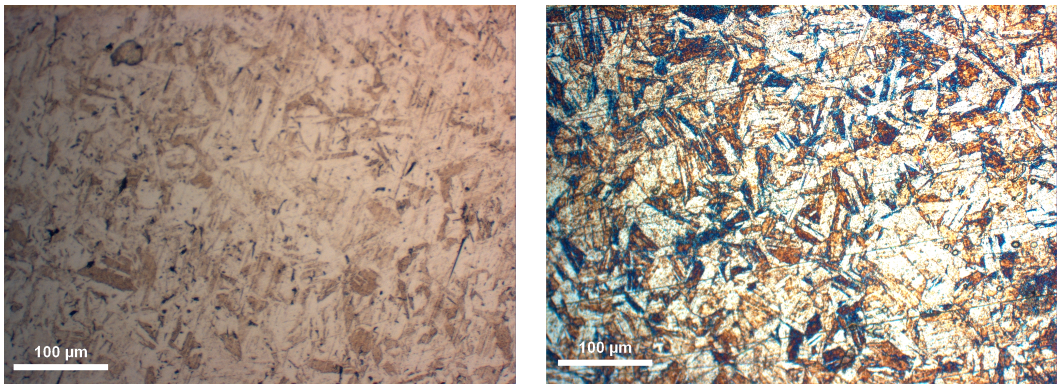

(a) *Micrograph of steel A after first cycle heat treating at T1=1000 °C/30min and air cooling. The microstructure consists of martensite (20X)*

(b) *Micrograph of steel A after first cycle heat treatment at T1 and tempering at T2=550 °C/60min and water cooling. The microstructure consists of martensite and carbides (20X)*

Figure 19: *Microstructure of steel (20X) after austenizing and tempering*

4.2.3 Transmission electron microscopy

TEM samples of specimens of steel A in austenitized state and tempered at 550 °C for different times was prepared as this was the temperature with the maximum hardness achieved for tempered samples.

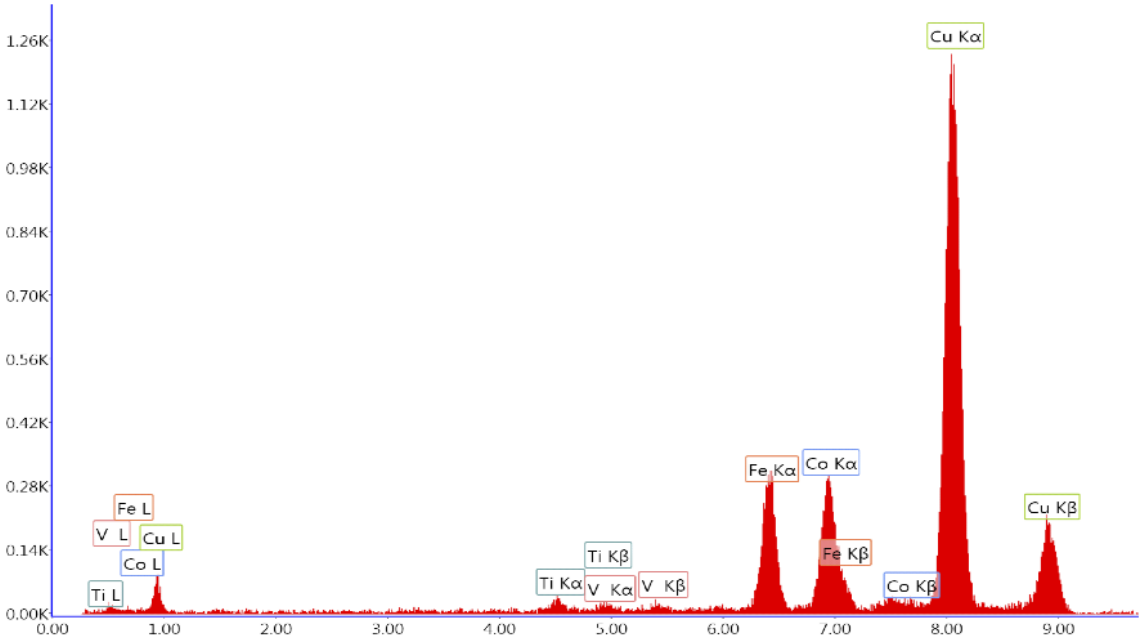

Figure 20: *EDS spectrum of copper grid holding the TEM replicas*

The TEM samples were prepared as carbon replicas carried by Cu grids. Therefore a Cu peak will be present on all the EDS spectrums performed on the samples in this study. The Cu peak originates from the copper grid holding the carbon replica, and should therefore be ignored in the following EDS spectrums. Fig. 20 show an EDS spectrum of the Cu grid. The Cu peaks are indicated in Fig. 20.

Note also that the EDS detector is newly installed and not yet adjusted to the microscope. Due to this the detector does not reach far enough in and Fe and Co radiation is picked up from the column. Thus, the Fe and Co peaks should with the intensity as in Fig. 20 should be ignored.

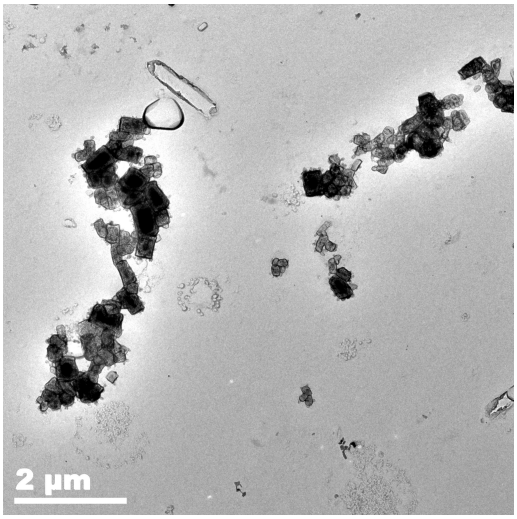

Figure 21: *Investigation of precipitates in steel A after single cycle heating T1*=1000 °C*/30min. Bright field image of carbon replica*

Fig. 21 show TEM bright field images of carbon replicas of the austenitized state of steel A. Large rectangular precipitates were found in the austenitized material.

Fig. 22a show a bright field image of a carbon replica of steel A tempered at T2=550 °C/2min with a magnification of 10k. The darker areas are precipitates. The precipitates are found in clusters and not spread in the matrix. Note that the size of the precipitates imaged is quite large, length of around 0.2 µm and also note that the shape of the precipitates is long and square. Fig. 22b show a bright field image of the same sample, but with a magnification of 100k. The precipitates found at this magnification have a diameter of around 40 nm. These precipitates were also found in clusters. In the upper right corner of the image (Fig. 22b) a selected area diffraction pattern of the precipitate indicated by the red arrow is inset. The selected area diffraction pattern (SAD) is indexed and reveals a (110) projection of a FCC-crystal with (111), (220) and (131) reflections closest to the origin. The shortest lattice spacing, between *(111)* reflections, is d= 0.16 nm (Eq. 2) and this gives a lattice parameter of a=0.45 nm.

Fig. 22c show an EDS spectrum of the particle indicated by a red arrow in Fig. 22b. The spectrum peaks are indicated with corresponding element. Note that the precipitate contain titanium. The cobolt and iron peaks are not accounted for due to the misalignment of the EDS detector as discussed above.

Fig. 23a is a bright field image with a magnification of 10k of steel A after tempering at T2=550 °C/15min. The image clearly show precipitates (dark spots) distributed evenly in the matrix. In Fig. 23b a bright field image of the same sample is taken with a 100k magnification. In the upper right corner is a selected area diffraction image of the precipitate indicated with a red arrow inserted. The diffraction image is

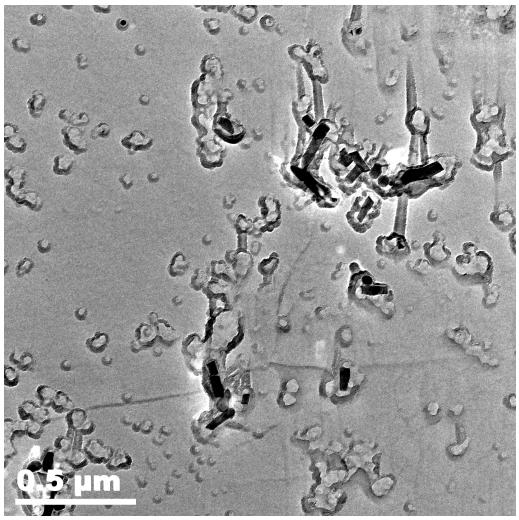

(a) *Bright field image steel A, double cycle condtion T2=550 °C/2min. Magnification 10k. Dark spots are precipitates*

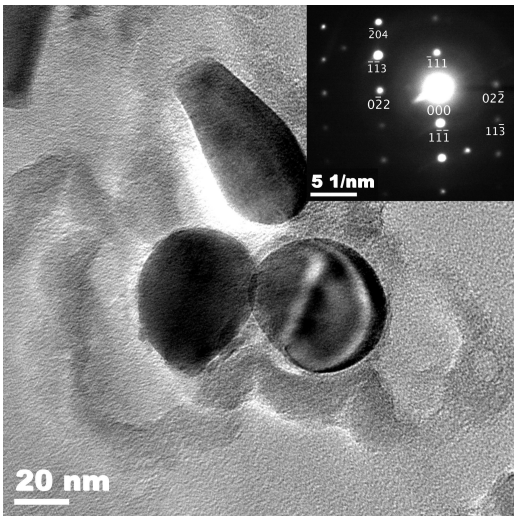

(b) *Bright field image steel A, double cycle condition T2=550 °C/2min. Magnification 100k. In the upper right corner the SAD pattern of the precipitate is inset*

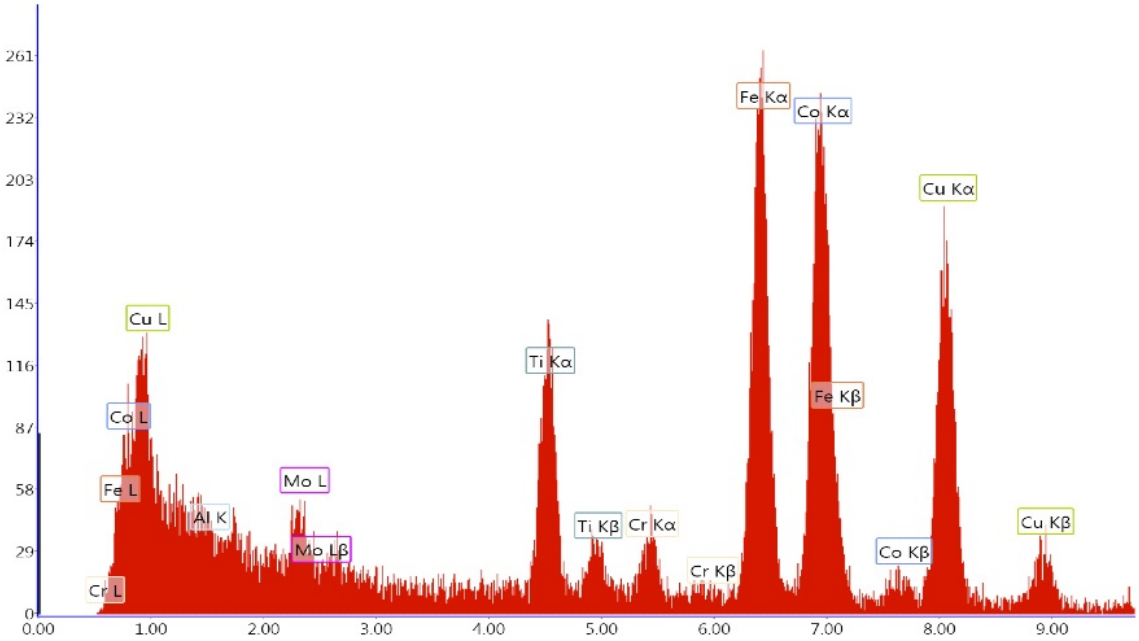

(c) *EDS spectrum of the particle indicated by the red arrow in Fig. 22b. Spectrum peaks are marked with corresponding element.*

Figure 22: *Investigation of precipitates in steel A after double cycle heating T2=550 °C/2min*

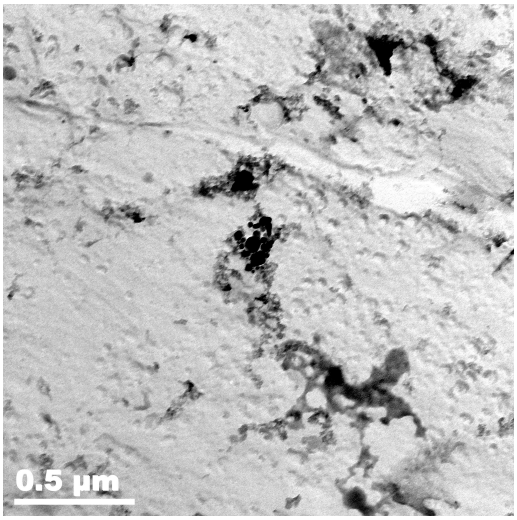

(a) *Bright field image steel A, double cycle condition T2=550 °C/15min. Magnification 10k. The dark spots are precipitates*

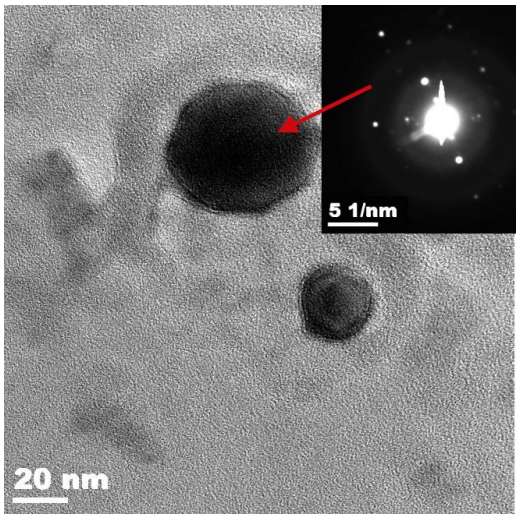

(b) *Bright field image steel A, double cycle condition T2=550 °C/15min. Magnification 100k. In the upper right corner the SAD pattern of the indicated precipitate is inset*

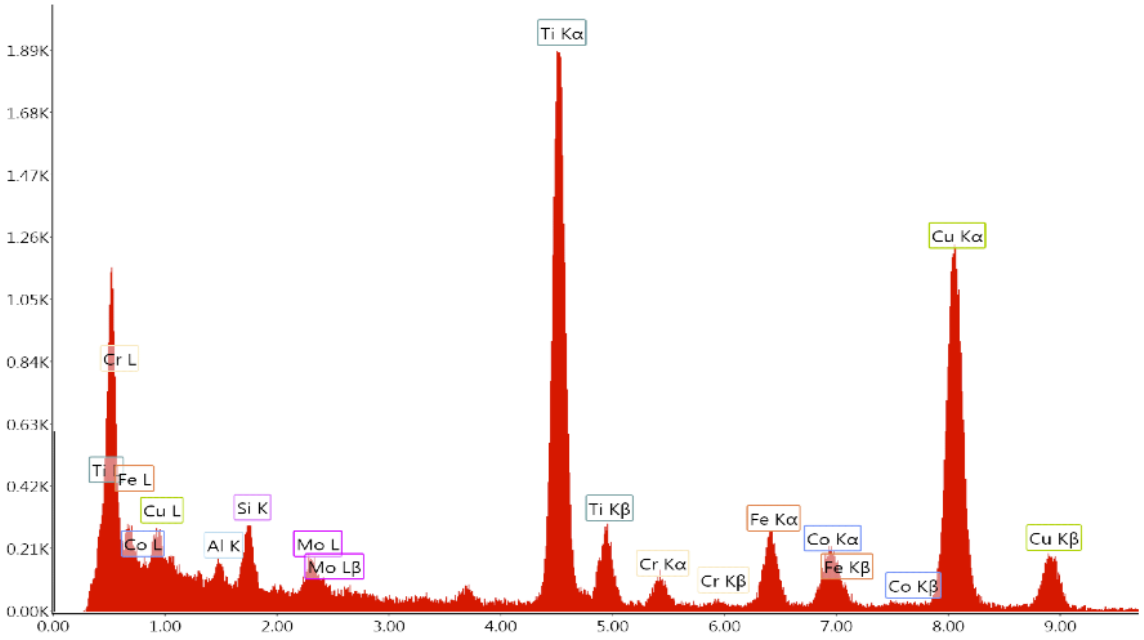

(c) *EDS spectrum of indicated by red arrow in Fig. 23b. Spectrum peaks are marked with corresponding element.*

Figure 23: *Investigation of precipitates in steel A after double cycle heating T2=550 °C/15min*

not indexed as some first order reflections are not visible, more tilting of the sample might have resolved this. The diameter of the precipitates is around 20-40 nm.

Fig. 23b show the EDS spectrum of the same precipitate as indicated in Fig. 23b. The spectrum peaks are marked with the corresponding element. Note that the precipitate contain titanium and molybdenum. Also note that the copper peak originates from the copper grid carrying the replica (as discussed in section 4.2.3).

Fig. 24a is a bright field image of a carbon replica of steel A tempered at T2=550 °C/20min with a magnification of 10k. The image show precipitates distributed in the matrix, the precipitates are the dark spots. Fig. 24b is a bright field image of a precipitate from the same sample as in Fig. 24a with a magnification of 100k. The diameter of the precipitate is around 30 nm and a selected area diffraction image of the precipitate is inserted in the upper right corner of the image. The diffraction pattern is indexed, and reveal that it is a (*110*) projection of a FCC-lattice with (220) and (111) reflections closest to the origin. The interplanar distance, d= 0.26 nm and the lattice parameter a= 0.45 nm.

Fig. 24c show the EDS spectrum of the precipitate in Fig. 24b. Note that the precipitate contains titanium and chromium and molybdenum. The copper peak, as discussed in section 4.2.3, originates from the copper grid carrying the replica.

Fig. 25a shows the carbon replica of the sample temperd at 550 °C for 30 minutes with a 10k magnification. The dark spots are precipitates. Note that the precipitates are dispersed throughout the matrix. In Fig. 25b is a closer view of some precipitates from the same sample as in Fig. 25a with a magnification of 100k. Note that the size of the precipitates are approximately 20 nm in diameter. In the upper left corner the SAD pattern of the precipitate indicated by the red arrow is inset in Fig. 25b. The SAD pattern is indexed and reveals a *(110)*-projection of a FCC-crystal with (220) and (111) reflections closest to the origin. The shortest distance between two planes is between the two *(111)*-reflections and the distance d= 0.24 nm and assuming it is the *(111)*-reflection, the lattice parameter becomes a= 0.41 nm. From the EDS analysis it is clear that the precipitate contain titanium and molybdenum (Fig. 25c).

Fig. 26a is an image of the carbon replica of steel A tempered at T2=550 °C/60min with a 10k magnification. The darker areas are precipitates. It is visible that the precipitates are found in clusters as well as distributed in the matrix. Fig. 26b is a closer view of the precipitates in the same sample taken with a 100k magnification. The darker areas are precipitates. Note that the size of the precipitate in the matrix is approximately 50 nm diameter. In the upper left corner the SAD pattern from the precipitate indicated with the red arrow is inset (Fig. 26b). Indexing of the diffraction pattern is indicated. Indexing the diffraction pattern reveals that it is a *(111)*-projection of a FCC-crystal with (220) reflections closest to the origin. The interplanar distance is d=0.16 nm and thus the lattice parameter a= 0.46 nm (Eq. 3). Fig. 26c shows the EDS spectrum of the same precipitate as indicated in Fig. 26b. Note that the precipitate contains titanium and molybdenum.

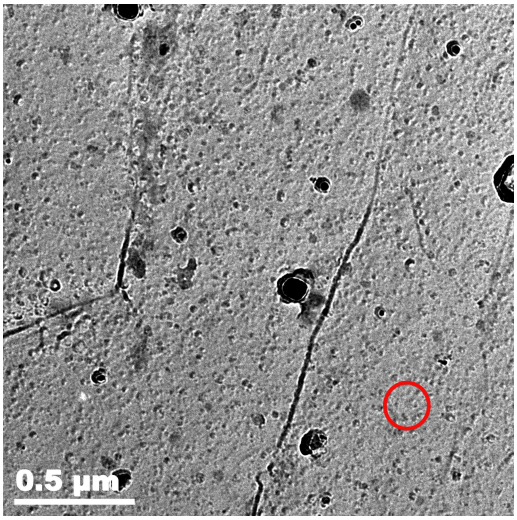

(a) *Bright field image steel A, double cycle condition T2=550 °C/20min. Magnification 10k. Dark spots are precipitates*

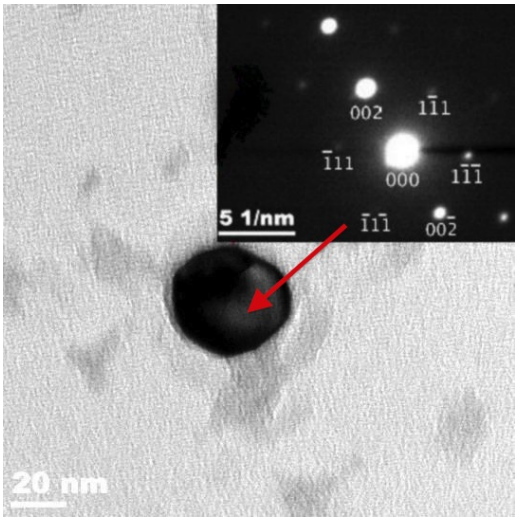

(b) *Bright field image steel A, double cycle condition T2=550 °C/20min. Magnification 100k. SAD pattern from precipitate indicated with red arrow is inset in upper right corner*

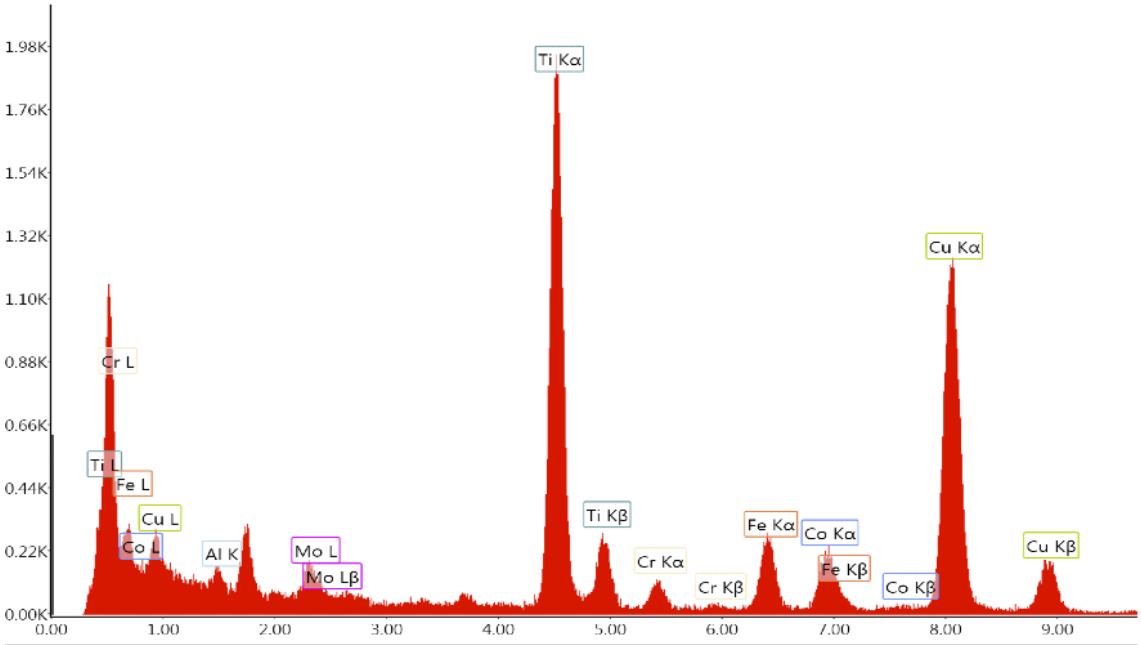

(c) *EDS spectrum of precipitate indicated with red arrow in Fig. 24b. Spectrum peaks are marked with corresponding element.*

Figure 24: *Investigation of precipitates in steel A after double cycle heating T2=550 °C/20min*

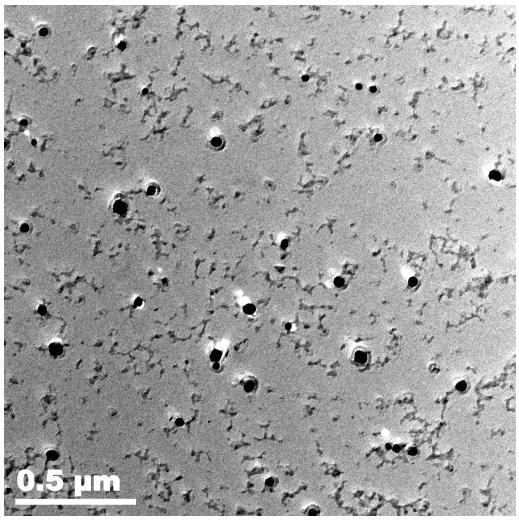

(a) *Bright field image steel A, double cycle condition T2=550 °C/30min. Magnification 10k. Dark spots are precipitates*

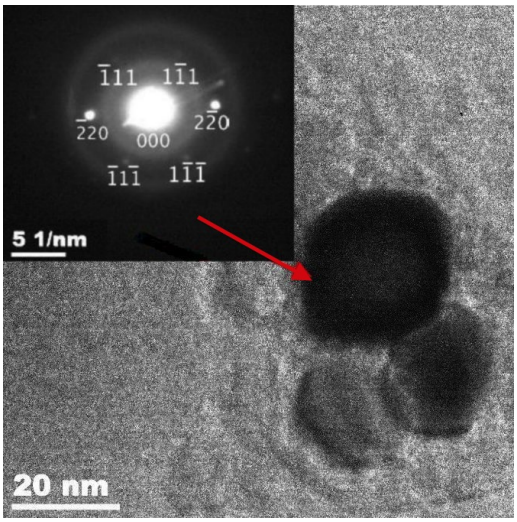

(b) *Bright field image steel A, double cycle condition T2=550 °C/30min. Magnification 100k. In the upper left corner the SAD pattern from the precipitate indicated with the red arrow is inserted.*

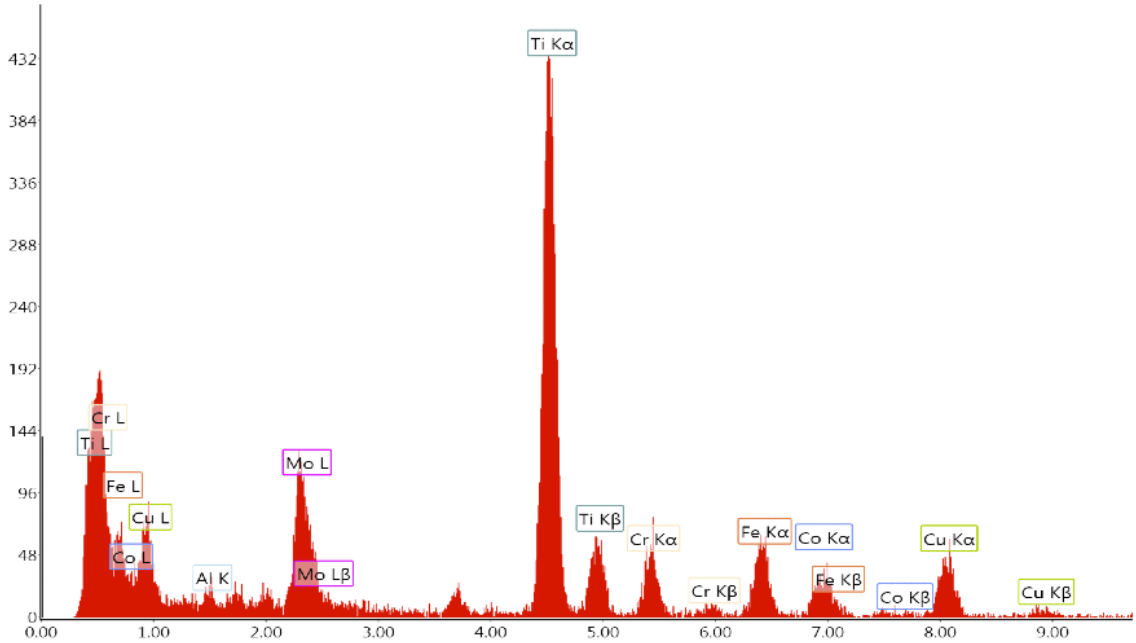

(c) *EDS spectrum of particle indicated by red arrow in Fig. 25b. Spectrum peaks are marked with corresponding element.*

Figure 25: *Investigation of precipitates in steel A after double cycle heating T2=550 °C/30min*

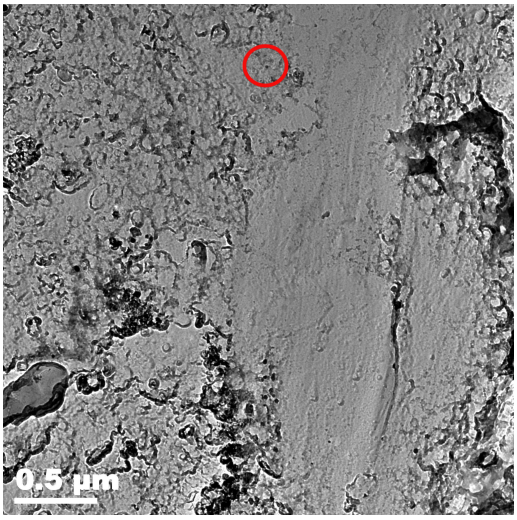

(a) *Bright field image steel A after tempering at T2=550 °C/60 min. Magnification 10k. Dark clusters are precipitates.*

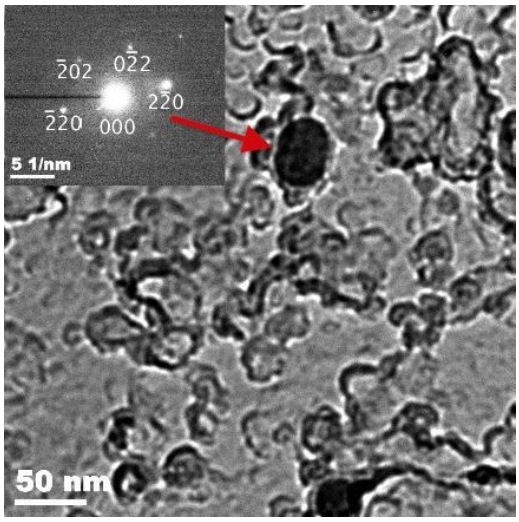

(b) *Bright field image steel A after tempering at T2=550 °C/60 min. Magnification 100k. The red arrow indicates the precipitate the SAD pattern in the upper left corner represents.*

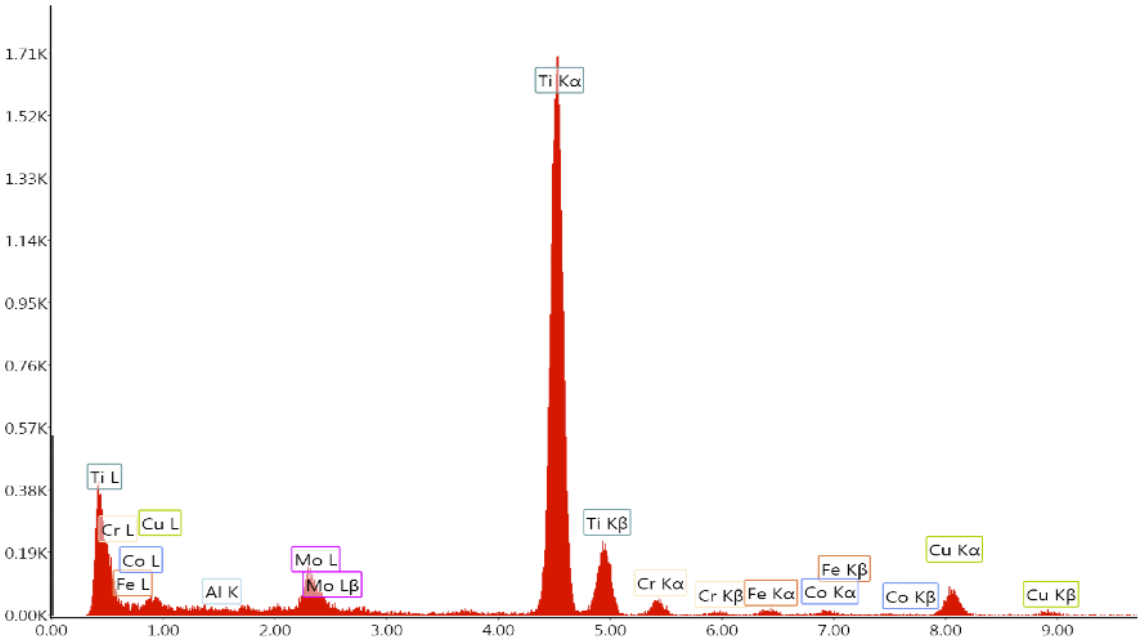

(c) *EDS spectrum of particle indicated by red arrow in Fig. 26b Spectrum peaks are marked with corresponding element.*

Figure 26: *Investigation of precipitates in steel A after double cycle heating T2=550 °C/60min*

4.3 Steel B

4.3.1 Hardness testing

After tempering at three different temperatures ($500, 550, 600\,^{\circ}\mathrm{C}$) with different holding times the hardness of the samples of steel B was measured. Hardness is tested in the middle of the samples. Tab. 7 shows the vickers hardness value (HV5) as well as the standard deviation (σ) for the different samples, all HV5 values are an average of ten readings (all HV5 readings as well as σ is tabulated in Appendix). The hardness of the austenitized state of steel B is also tested and presented in Tab. 7.

Table 7: *Vicker's hardness value as a function of holding time at temperatures T2=*500 °C*,* 550 °C *and* 600 °C *for steel B. Each HV5 value is an average of ten readings (all readings are presented in Appendix)* σ *represents the standard deviation of the readings*

t2	austenitized		T2=500 °C		T2=550 °C		T2=600 °C	
[min]	[HV5]	σ	[HV5]	σ	[HV5]	σ	[HV5]	σ
0	338	6	-		-		-	
1	-		308	5	292	5	299	5
2	-		305	7	301	5	301	7
10	-		301	4	288	3	306	3
11	-		297	3	296	2	304	6
12	-		297	5	303	4	308	5
13	-		299	7	305	3	307	4
14	-		304	5	306	3	307	3
15	-		306	2	311	5	309	3
16	-		313	4	311	3	314	5
17	-		316	4	312	3	306	2
18	-		311	4	315	3	306	4
19	-		303	7	311	3	305	4
20	-		300	5	307	4	301	3
30	-		298	5	301	4	297	4
60	-		295	3	299	3	293	4

Fig. 27 shows the hardness of the samples tempered at 500 °C. Note that there is a significant drop in the hardness from that of the austenitized state to that of the 1 minute tempered state. Note also that the hardness of the sample tempered for 60 minutes is the lowest measured with a hardness of 295 HV5 (Fig. 27). Maximum hardness for the samples tempered at 500 °C is achieved after 17 minutes of tempering with a hardness of 316 HV5.

Fig. 28 show the hardness in the samples of steel B tempered at 550 °C. There is a drop in hardness from that of the austenitized state to that of the 1 minute tempered state. Note that from the 2 minute tempered state to the 10 minute tempered state there is also a drop in the hardness (Fig. 28). The maximum hardness of the tempered samples is measured for the sample tempered for 18 minutes with a

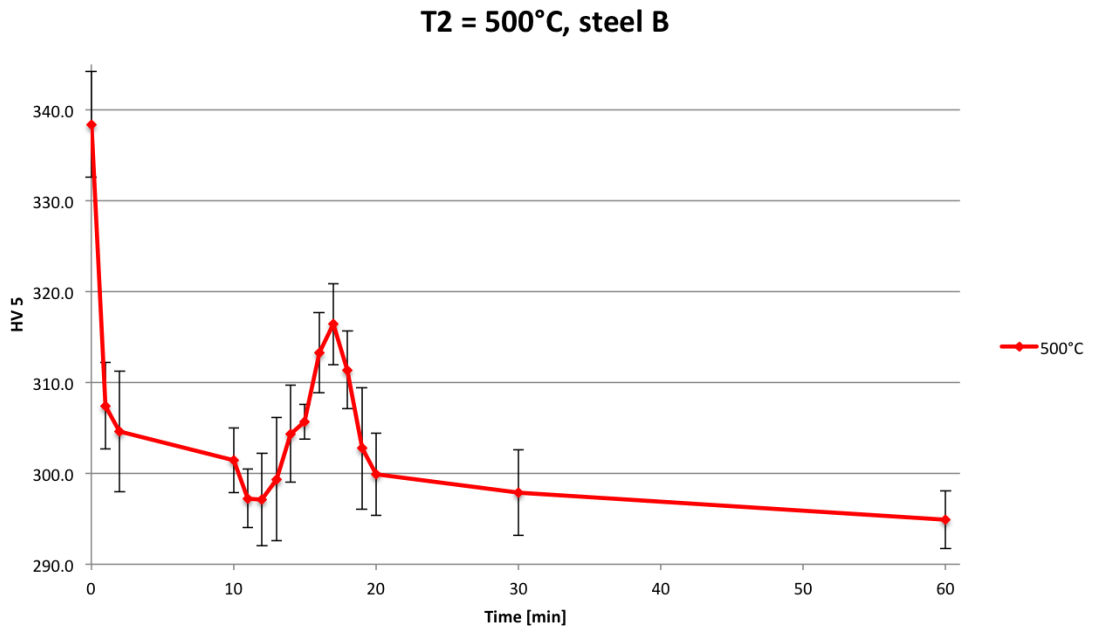

Figure 27: *HV as a function of time at T2=500 °C for steel B, average of ten readings*

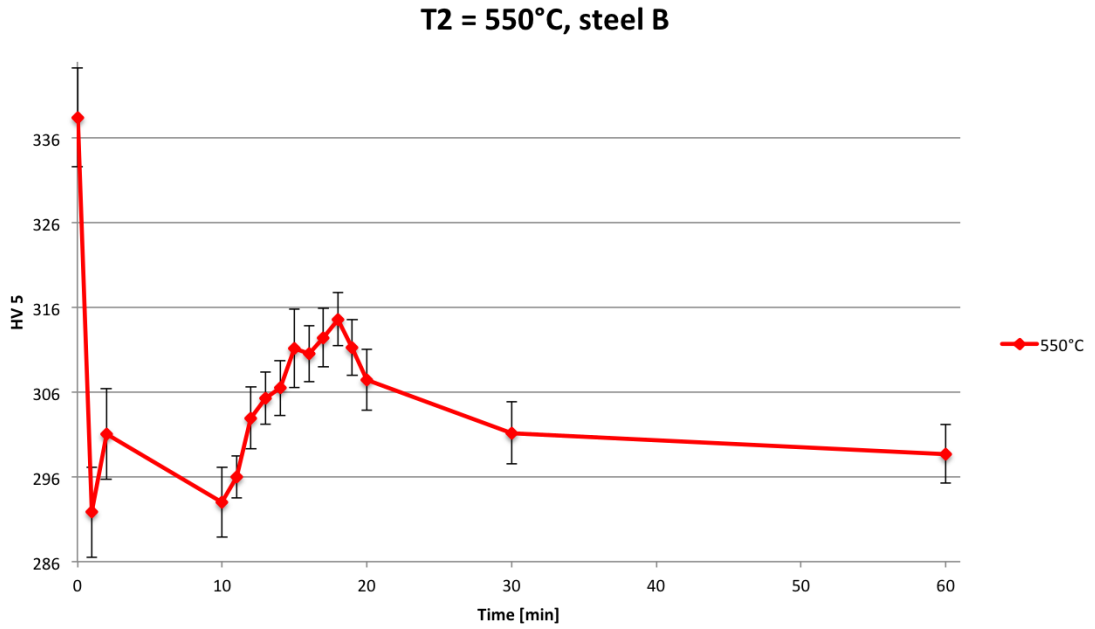

Figure 28: *HV as a function of time at temperature T2=550 °C for steel B, average of ten readings*

hardness of 315 HV5. The lowest hardness measured is that of the 1 minute tempered sample with a hardness of 292 HV5. Note that this is the lowest hardness measured for all the tempered samples of steel B for all temperatures (500 °C, 550 °C, 600 °C) investigated. The hardness decreases from the sample tempered for 20 minutes at 550 °C towards tempering time of 60 minutes (Fig. 28).

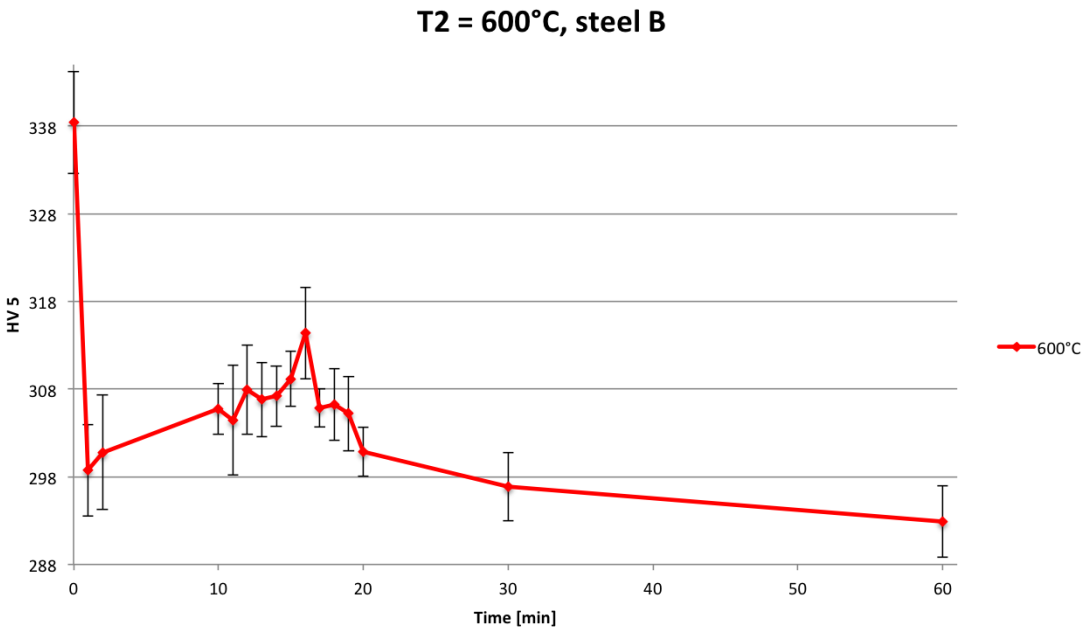

Figure 29: *HV as a function of time at T2=*600 °C *for steel B, average of ten readings*

Fig. 29 show the hardness for the samples of steel B tempered at 600 °C. There is a drop in hardness from that of the austenitized state to that of the 1 minute tempered state. From the 2 minute tempered state towards 16 minutes tempered state the hardness is increasing. The maximum hardness of the tempered samples is measured after 16 minutes tempering with a hardness of 314 HV5. The lowest hardness is achieved for the sample tempered for 10 minutes at 550 °C with a hardness of 288 HV5.

Note that the maximum hardness achieved for the tempered samples of steel B is that of the sample tempered at 500 °C for 17 minutes with a hardness of 316 HV5. The samples tempered at 600 °C reaches it hardness maximum after 16 minutes with a hardness of 314 HV5, this is the earliest hardness maximum measured compared to that of the samples treated at 500 °C and 550 °C which reaches their maximums after 17 minutes and 18 minutes respectively with hardness 316 HV5 and 315 HV5 respectively.

Table 8: *Key results from hardness testing of tempered samples of steel B. [min] columns indicates tempering times and the variation in hardness column indicates how much the hardness varies over all the samples tempered at the same temperature*

Tempering temperature	**Max.hardness, tempered state**		**Min.hardness, tempered state**	
	[HV5]	t2 [min]	[HV5]	t2 [min]
500 °C	316	17	295	60
550 °C	315	18	288	10
600 °C	314	16	293	60

4.3.2 Metallographic examination

Fig. 30a show the microstructure of the austenitized state of steel B and Fig. 30b show the microstructure the double cycle sample with T2=550 °C/60min for steel B. Martensite structure is visible for both states, but for the tempered sample the martensite areas are darker, which may indicate that it is tempered martensite and the brighter areas are fresh martensite.

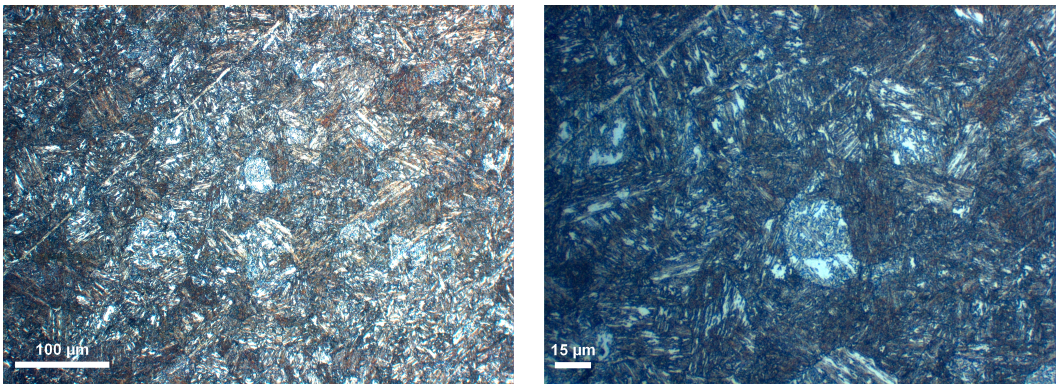

(a) *Micrograph of steel B, austenitized state (T1=1000 °C/30min. Magnification 20X and the microstructure consist of martensite*

(b) *Micrograph of steel B, double cycle heat treated T2=550 °C/60min. Magnification 50X and the microstructure consist of tempered and fresh martensite.*

Figure 30: *Light microscopy of steel B after austenitizing and tempering.*

4.3.3 Transmission Electron Microscopy

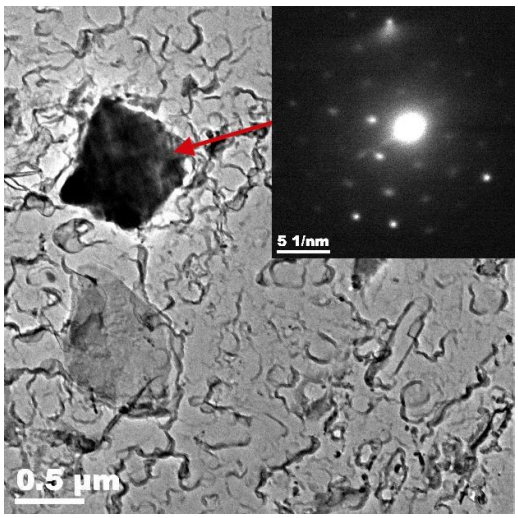

Figure 31: *Bright field image of steel B, austenitized state (T1=1000 °C/30min). Magnification 10k. SAD pattern of indicated precipitate is inset in upper right corner*

Fig. 31 show a bright field image of a carbon replica of the austenitized state of steel B with a magnification of 10k. The precipitate has a diagonal size of around 1 µm, which is quite large. In the upper right corner the selected area diffraction image of

the precipitate indicated by the red arrow is inset. EDS show that the precipitate contains silicone and oxygen. The precipitate is not important for the scope of this work. No carbides were found in the austenitized state of steel B.

Fig. 32a show a bright field image of steel B tempered at 550 °C for 2 minutes with a magnification of 10k. Note that the darker areas in the image is clusters of precipitates. Some precipitates are also seen distributed in the matrix.

Fig. 32b show a bright field image of steel B taken with a magnification of 100k. In the upper right corner the selected area diffraction image of the precipitate indicated by the red arrow is shown in Fig. 32b. The diffraction image is indexed, revealing a (*111*) projection of a FCC-lattice with (220) reflections closest to the origin. The interplanar distance of the (*220*) planes is d=0.35 nm and the lattice parameter a=1.01 nm.

Fig. 32c show the EDS spectrum of the precipitate indicated in Fig. 32b. Note that the precipitate contains chromium.

Fig. 33a show a bright field image of the carbon replica of steel B after tempering at 550 °C for 60 minutes with a magnification of 10k. The darker areas in the image are precipitates. Most precipitates are found in clusters, but also some precipitates visible in the matrix.

Fig. 33b show a bright field image with a magnification of 10k of precipitates in steel B after tempering for 60 minutes at 550 °C. The precipitates have a diameter of around 40 nm. The selected area diffraction image of the precipitate indicated by the red arrow (Fig. 33b) is indexed and inset in the upper right corner of the Fig. 33b. The indexing indicates that the diffraction image is a (*111*) projection of a FCC-crystal with (220) reflections closest to the origin. The interplanar distance, d= 0.39 nm and the lattice parameter a= 1.09 nm.

The EDS spectrum of the precipitate indicated in Fig. 33b is shown in Fig. 33c. Elements corresponding to the spectrum peaks are indicated. Note that the precipitate contains chromium and molybdenum.

Also note that the precipitates in the 60 minutes tempered state of steel B are larger than that of the 2 minutes tempered sample.

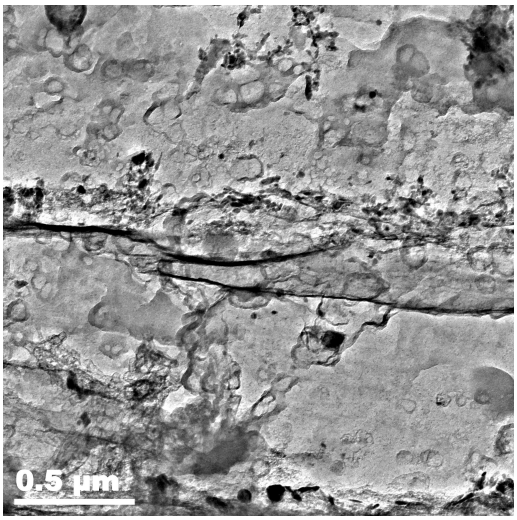

(a) *Bright field image steel B, double cycle heat treated at T2=550 °C/2min. Magnification 10k. The dark spots are precipitates*

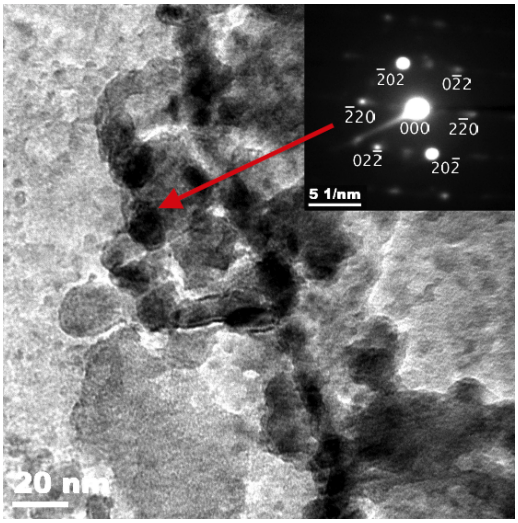

(b) *Bright field image steel B, double cycle heat treated at T2=550 °C/2min. Magnification 100k. SAD pattern of indicated precipitate inset in upper left corner*

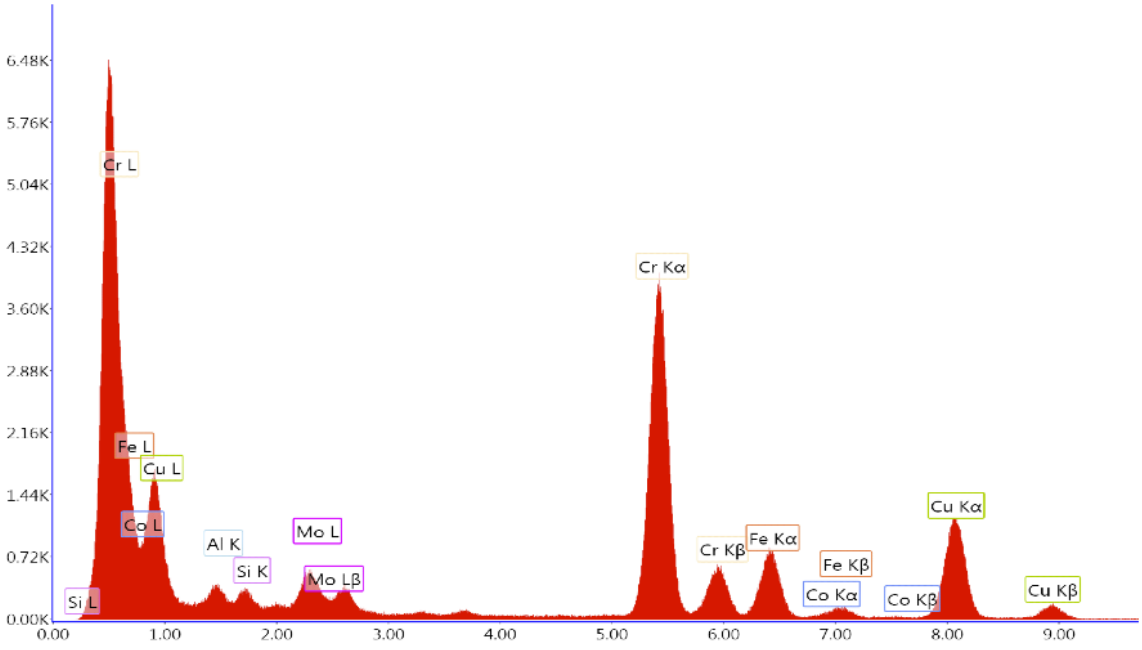

(c) *EDS spectrum of particle indicated by red arrow in Fig. 32b. Spectrum peaks are marked with corresponding element.*

Figure 32: *Investigation of precipitates in steel B after double cycle heating T2=550 °C/2min*

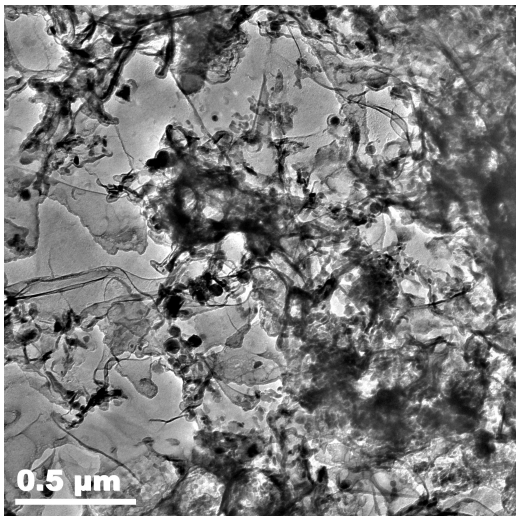

(a) *Bright field image steel B, double cycle heat treatment at T2=550 °C/60min. Magnification 10k. The dark spots are precipitates.*

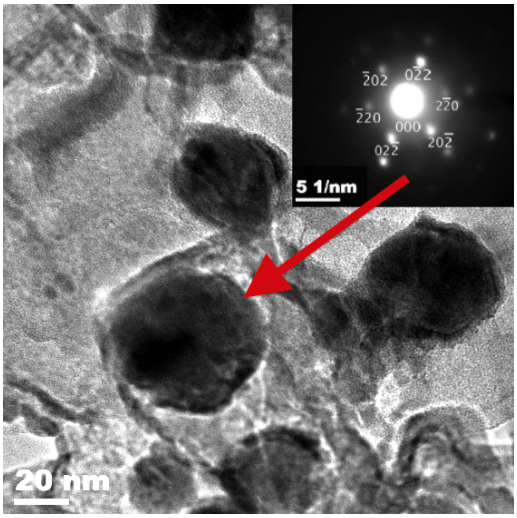

(b) *Bright field image steel B, double cycle heat treatment at T2= 550 °C/60min. Magnification 100k. In the upper right corner an indexed SAD pattern from the precipitate indicated by the red arrow is inset*

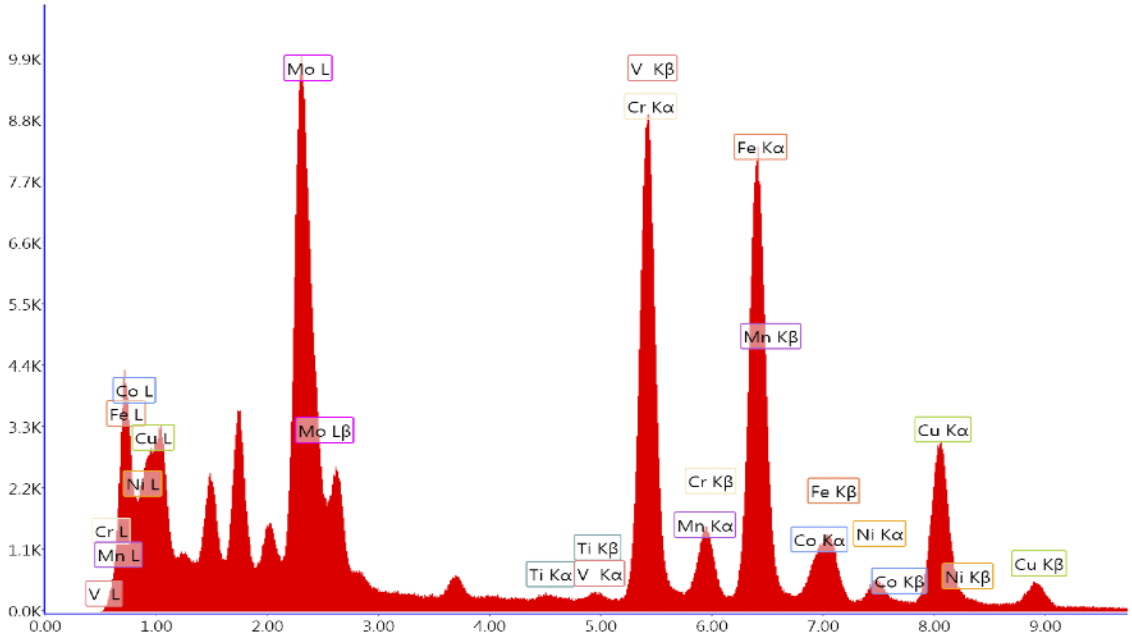

(c) *EDS spectrum of particle indicated by red arrow in Fig. 33b. Spectrum peaks are marked with corresponding element.*

Figure 33: *Investigation of precipitates in steel B after double cycle heating T2=550 °C/60min*

5 Discussion

5.1 Steel A

5.1.1 Type of carbides

From the lattice parameters calculated from the SAD patterns of precipitates and the chemical analysis done with EDS (Section 4.2.3) some conclusions can be made as to which type of precipitates are found.

In the samples tempered for 2 minutes a precipitate with lattice parameter a= 0.45 nm was found. This value only deviates 4.2% from the lattice parameter of cubic TiC (a=0.43176 Tab. 4 [18]). From the chemical analysis of the precipitate it is seen that it contains molybdenum and titanium. It is thus likely that the precipitate is of MC type and the deviation in lattice parameter is due to Mo also present. The precipitate can be written as (Ti,Mo)C. Ladanova also found that the deviation in the lattice parameter from that of TiC was due to the presence of Mo [4].

In the sample tempered for 20 minutes the lattice parameter for a precipitate is also found to be a=0.45 nm and this again is a 4.2% deviation from that of TiC. The precipitate contains much more titanium than in the two minute tempered sample but it also contains molybdenum. The precipitate is of the type MC and in this case can be written as (Ti,Mo)C.

The sample tempered for 30 minutes has a carbides with lattice parameter of a= 0.41 nm which again is very close to that of TiC, only 5% deviation. From the EDS analysis performed on the precipitate it is found that it contains titanium and molybdenum, it is thus likely that the precipitate is of type (Ti,Mo)C.

Finally for the sample tempered for 60 minutes the lattice parameter was found for a carbide, a= 0.46 nm. Again very close to that of TiC (Tab. 4 [18]) with a deviation of 6%. The chemical analysis show that the precipitate contain titanium and molybdenum. The precipitate must therefore be of type (Ti,Mo)C.

This reveals that titanium carbides was found in all tempered samples of steel A which was expected for steel A due to titanium's high affinity to carbon. TiC carbides require much more carbon than $M_{23}C_6$, and therefore, if the amount of titanium in the steel is sufficient, all the carbon can be involved in precipitation of titanium carbides and prevent the precipitation of chromium carbides. Thus, all the chromium will stay in solid solution and there will be no chromium depletion in the vicinity of grain boundaries and the corrosion properties are expected to be kept. In the sample of steel A that was single cycle heat treated there was not found any carbides. This is because very little precipitation occurs in SMSS during cooling since the steel remains austenitic down to very low temperature and the precipitation rate of carbides is very low in austenite. A second heat cycle is necessary in order to get precipitation as precipitation only occurs by heating the material after the martensite transformation.

5.1.2 Precipitation sequence

In the single cycle heat treated (T1=1000 °C/30min) sample of steel A (Fig. 21), large rectangular precipitates in clusters are found. Steel A containes nitrogen and carbon, and since both are carbide and nitride formers, the particles in clusters could either be carbides, nitrides or carbonitrides. But based on the particle shape, which was rectangular, it can be concluded that the particles probably are nitrides because nitrides are always nearly rectangular particles with sharp corners. The nitrides are not interesting in the context of this thesis. Thus, carbides were not found in the austenitized state of steel A, and precipitation of carbides is only achieved by heating of the material after the martensite transformation. Thus, the carbides found in steel A for the tempered samples are formed during tempering, and the development in size and distribution during tempering is possible to compare for the different tempering times.

From the graphs showing the hardness of the samples as a function of tempering time t2 (Fig. 16, 17, 18) it is seen that for all tempering temperatures investigated in this experiment there is a drop in hardness from the single cycle state of the steel to that of the 1 minute tempered state of the steel. This is due to the loss of the primary hardening as the carbon that is in solid solution is now being used for the formation of carbides. But after only one minute of tempering there is no secondary hardening effect for neither of the temperatures explored as the formed carbides are too small and too few to make a hardening contribution. As the tempering time increases, the carbides grow and the density of carbides increases and a secondary hardening effect is observed. TEM investigation of the samples tempered at 550 °C shows a development in carbide size and distribution as the tempering time changes.

In the sample tempered for 2 minutes at 500 °C small titanium carbides are found by the use of TEM (Fig. 22b). The hardness of the samples start increasing after 2 min tempering for all the three temperatures explored.This indicates that the density and size of the carbides in the material start to become large enough to make a hardness contribution. From the TEM images of steel A it is possible to see the change in size and distribution of the carbides as the tempering time change. For the sample tempered for 15 min, which is the one closest to the hardness peak (t2=12 min), and investigated with TEM particles were found as single particles or in clusters. The precipitates found distributed in the matrix are larger than those found in the 2 min sample. It is the carbides that are found distributed in the matrix that are associated with the secondary hardening effect as the size and distribution of the carbides are of importance for the effect. For instance PWHT is used to soften the material and is associated with the precipitation of clusters of $M_{23}C_6$ carbides. It is possible that the detected precipitates have formed on grain boundaries and inside the grains. It is difficult to talk with certainty about the location of the precipitates as it was difficult to distinguish between prior austenite grain boundaries and martensite subboundaries in the carbon replica. The carbides could be located at the grain boundaries, but since they are so small (20-40nm) they could easily float away during the final etching of the replica. The small single precipitates found evenly distributed on the carbon replica is due to precipitation in the interior of grains. The larger precipitates found in clusters at grain boundaries

nucleate earlier and thus, are larger. The precipitates along grain boundaries grow faster as the grain boundary is a diffusion canal for Ti. It is possible that the larger precipitates are in a cluster due to agglomeration during the final etching of the sample preparation. On the other hand, the replica might show the correct positioning of the carbides and thus indicating that carbides can form on both grain boundaries and inside grains. It is likely to believe that the positioning shown is correct as the hardness of the material has increased.

As the precipitation of carbides is a time and temperature dependent mechanism the maximum hardening is achieved for shorter tempering times for the sample tempered at 600 °C and the sample tempered at 500 °C needs longer time to reach the secondary hardening maximum. It is also interesting to note that the maximum hardness found for steel A in tempered condition is above the primary hardness of steel A in quenched condition (austenitized at T1=1000 °C/30min), which is not expected as tempering is associated with softening of the material as carbon in solid solution gives a higher hardening effect than carbides do. The hardness changes during tempering are very dependent on carbon content, and increase in hardness has been observed in the temperature range $50 - 150$ °C for steels containing more than 0.4%C due to precipitation of ϵ-carbide that strengthens the martensite [9]. Solheim [13] also experienced an increase in hardness for samples tempered at 500 °C for titanium alloyed SMSS. However, the overall trend is softening as the tempering temperature is raised.

A secondary hardening peak is observed for all temperatures, and also a drop in hardness is observed as the tempering time goes over that of the peak. This is due to a coarsening of the carbides with increased tempering time. The carbides are no longer small enough or finely dispersed enough to preserve the same hardening effect. From TEM images of samples tempered for 30 min and 60 min at 550 °C, it is seen that the precipitates have grown larger and the distribution is not as fine as for shorter tempering times (Fig. 25a, 26a). But some smaller carbides are found for the two samples when increasing the magnification to 100k (Fig. 25b, 26b). This indicates that precipitation of new carbides continues during tempering and that larger carbides are older. The coarsening of the older carbides decreases the hardening effect, and the precipitation of new carbides contributes to the secondary hardening effect. But due to the coarsening of the precipitates and thus increasing density of carbides in the matrix the hardening is no longer so prominent although smaller carbides are still present in the matrix.

For the sample tempered at 500 °C, a decrease in hardness is seen for tempering times longer than 30 minutes (Fig. 16). This may indicate that the precipitation of new carbides is not occuring at all or to the same degree as for the other temperatures. Only coarsening of the precipitates is happening, and thus a decrease in the hardness of the steel takes place.

5.2 Steel B

5.2.1 Type of carbides

In the sample tempered for 2 min, a high density of carbides in clusters was found along what could be previous austenite grain boundaries. The lattice parameter of on of the precipitates in a cluster was found to be a=1.01 nm (Eq. 3). The chemical composition of the same precipitate was found by the means of EDS and showed that it mostly contains chromium. The lattice parameter of a $M_{23}C_6$ carbide is a=1.0650 nm [18]. Accordingly it is likely to believe that the precipitates are of the $M_{23}C_6$ type.

For the sample tempered for 60 min the lattice parameter of a carbide was found to be a= 1.09 nm (Eq. 3). From the EDS spectrum of the particle in the sample tempered for 60 min it can be seen that the precipitate contain molybdenum, chromium and iron. It is likely to assume that the precipitates found in clusters in steel B after 60 min tempering is of the type $M_{23}C_6$ and that the deviation in the lattice parameter found is due to the other elements present and that the carbide can be written as $(Cr, Mo,Fe)_{23}C_6$.

No carbides were found in the austenitized state of steel B as was expected. This indicates that a second heat cycle after the martensitic transformation is necessary in order to get precipitation of carbides. In both tempered samples investigated with TEM of steel B chromium carbides were found.

5.2.2 Precipitation sequence

In the single cycle heat treated (T1=1000 °C/30min) sample of steel B (Fig. **??**), large silicon precipitates were found, but no carbides were found in the austenitized state of the material. Precipitation of carbides is only achieved by heating of the material after the martensite transformation.

The results from the hardness testing (Fig. 27, 28, 29) show a secondary hardening peak for all temperatures (500 °C-600 °C) tested for steel B. A drop in hardness is observed for all temperatures tested from the quenched state of the material (T1=1000 °C/30min) to the 1 minute tempered samples. The reason for the drop in hardness is that the primary hardening is lost as the carbon in solid solution is used for carbide precipitation. For the samples tempered at 550 °C and 600 °C there is an increase in hardness after 2 min tempering, but for the sample tempered at 500 °C there is a decrease in hardness up to 12 min tempering. This indicates that the precipitation of carbides is slower at 500 °C. It is possible that carbide precipitation is starting already after 1 min of tempering, but as the carbon is taken from solid solution to carbide precipitation there is no net hardening effec,t before the carbide density is high enough. Other reasons for the continuous drop in hardness can be that carbon in solid solution gives a higher contribution to hardening than carbides do, or that dislocations are annihilated by annealing. The annihilation of dislocations is slow due to the high chromium content [20]. A drop in hardness from 2 min to 10 min tempering is also seen for the sample tempered at 550 °C, this could

be for the same reasons as for the samples tempered at 500 °C, or it could be related to the heating method used. The 2 min sample was heated with Smitweld Thermal Cycle Simulator and the 10 min sample was heated with Nabertherm C290 oven. The difference in heating time to the tempering temperature is large, with 5 seconds for Smitweld and 5 minutes for Nabertherm (Fig. 15). A higher hardness for the samples treated in Nabertherm was expected, as the five minutes heating time extra at temperatures below t2 might allow for some precipitation during heating. This would result in finer precipitates when the tempering temperature is reached and more sites for carbide nucleation. Thus, it is likely to assume an increase in the hardness of the material. An explanation to the drop in hardness could be that iron carbides are formed and thus, consuming some of the carbon in solid solution, lowering the hardness. The phase diagram for iron-chromium show that iron carbides is a possible precipitate (Fig. 1).

From investigation with light microscope it is found that the single cycle heat treated sample consists of fresh martensite and some stable austenite, but it is difficult to distinguish between untempered fresh martensite and retained austenite under an optical microscope. To better distinguish between the phases colour-etching techniques could be helpful. The double cycle heat treated sample contains both fresh and tempered martensite and precipitates. Difference in etching response is seen from the 1000 °C single cycle condition to the 550 °C/60 min double cycle condition, probably reflecting the presence of secondary hardening precipitates (Fig. 30).

For all tempering temperatures tested for steel B a secondary hardening peak is found, but the hardness peak does not exceed the hardness of the single cycle heat treated sample, as was the case for steel A. This indicates that the hardening effect of titanium carbides is larger than that of chromium carbides.The hardness peak is reached within 18 minutes of tempering for all temperatures explored for steel B. The precipitation, and thus, secondary hardening, is a time and temperature dependent process and for the samples tempered at 600 °C the hardness peak is reached faster than for the samples treated at lower temperatures. The sample treated at 600 °C reaches the maximum hardness first (Tab. 8) but has a lower hardness maximum than for the two other temperatures, although the variation is only 2 HV5.

In the sample tempered at T2=550 °C/2min investigated with TEM, clusters of small carbides were found. Very few carbides were found outside of clusters and the carbides found were very small. This explains why the hardness is so low for the 2 min tempered sample. The carbides are not large enough or evenly distributed enough to make a hardness contribution. Single carbides distributed in the interior of grains is associated with the hardening effect. Clusters of $Cr_{23}C_6$ is associated with softening of the material, and it is also what is found to be the precipitation mechanism during PWHT [17].

In the sample tempered at T2=550 °C/60min clusters of precipitates are found throughout the sample. The precipitates are mostly found in clusters along what could be previous austenite grain boundaries. In Fig. 33b is bright field image with increased magnification of 60 min tempered sample and the size of the precipitates is found to be 20-40nm. Ladanova [4] found that the precipitation of

the non-titanium alloyed steel consists mainly of $M_{23}C_6$ on previous austenite grain boundaries. Ladanova [4] also found that the $M_{23}C_6$ precipitation peak temperature was 650 °C and that the particles consisted mainly of chromium and iron, but also of molybdenum and silicon. According to the the textbook of Folkhard [6], $M_{23}C_6$ generally contains 42-65% chromium. Precipitates of this type ($M_{23}C_6$) along previous austenite grain boundaries is known to soften the material. As discussed in section 2.1.3 carbides start to coarsen at higher temperatures and new carbides form and thus continues to take carbon out of solid solution and thus hardness decreases and the coarsened precipitates are no longer finely dispersed enough to harden the material. After the secondary hardening peak there is a decrease in hardness for all tempering times longer than that associated with the maximum hardness (Fig. 27, 28, 29). This is probably due to a coarsening of the carbides.

Precipitates in clusters were mainly found in the TEM analysis of steel B and in both tempered samples the precipitates were of the type $M_{23}C_6$. But also smaller precipitates in the interior of grains were found. Thus, a binodal distribution of carbides is found in steel B as was also found in steel A. Larger carbides were found in clusters along grain boundaries and smaller carbides were found distributed in the grains. It is the smaller carbides that are associated with the secondary hardening effect. Carbides in the interior of the grains were more difficult to find in steel B than in steel A, even after 60 min tempering where the precipitate size is quite large. This indicates that there are fewer and smaller carbides contributing to the secondary hardening effect in steel B, which is also reflected in the hardness results.

It is worth to mention that the secondary hardening effect is not a wanted effect and it is not used on purpose to harden the material. The negative effect of second heat cycle both to 500 °C and to 750 °C has been observed by Solheim [13] in his phd work and Solheim also found that a post weld heat treatment cycle may eliminate the negative effect of the second cycle to a large extent. In the cases where PWHT is needed it is applied to soften the material. It is also worth mentioning that chromium depletion around the precipitates can be a problem in SMSS that are not titanium stabilized (as steel A is) and can lead to a decrease in corrosion resistance as the local chromium content may drop below 11.5wt% [4]

6 Conclusion

In this work secondary hardening has been explored for two high grade SMSS, one alloyed with Ti (steel A) and one not (steel B). The experiment included single and double cycle heat treatment of both steels. The resulting microstructures were characterized by standard metallographic techniques, hardness testing and TEM.

It was found that:

- Secondary hardening is observed in both steel A and B for all second cycle temperatures tested $500 - 600\,^{\circ}\mathrm{C}$.
- The secondary hardening effect is higher in steel A than in steel B.
- In steel A the secondary hardening peak exceeds the hardness of the as quenched state of the steel.
- No carbides were found in steel A and steel B in quenched condition from $1000\,^{\circ}\mathrm{C}$.
- Carbide type found in the two steels was determined from SAD patterns and chemical analysis with EDS of carbides.
  - In steel A the carbides were cubic with a=0.41-0.46 nm which corresponds to that of TiC.
  - In steel B the carbides were cubic with a lattice parameter a=1.01-1.09 nm which corresponds to that of $Cr_{23}C_6$.
  - EDS analysis shows that TiC contains Mo and can be written as (Ti,Mo)C and that $Cr_{23}C_6$ primarily contain Fe and Mo and can be written $(Cr,Mo,Fe)_{23}C_6$.
- There is a binodal distribution of precipitates in both steels. Small precipitates are found in the interior of grains and larger precipitates are found at grain boundaries. It is the smaller precipitates that are assumed to give the hardening effect.
- Correlation between hardness results and carbide observations with TEM.

The present study was conducted using two specific SMSS steel grades and specific heat treatments. The behavior of other steels with slightly different alloy compositions and heat treatments may be quite different both for the secondary hardened condition and the quenched condition.

7 Further Work

To better investigate the tempering effect in multipass welding shorter tempering times should be tested for both steel A and steel B.

It would also be of importance to investigate the effect of the difference in heating from the two heating methods used in this experiment. By tempering two samples with the same time the precipitation in the two could be compared and thus the possibility of precipitation during heating in Nabertherm on temperatures below the actual tempering temperature could be mapped. It is clear that the difference in heating affects the results.

It would also be of importance to investigate more tempered samples of steel B with TEM to se if other types of precipitates are present in the steel other than what was found in this experiment.

It would be interesting to heat treat steel A and steel B with more realistic heat cycles, i.e. times and temperatures reflecting industrial practice for two cycle welding welding and for PWHT. Then precipitation in 13Cr SMSS in the state it is in use could be investigated more thoroughly.

Lastly experiments on the hydrogen trapping effect of carbides in SMSS would be interesting to investigate further. Solheim [13] and Rosenquist [7] has done some investigation on this matter already.

Acknowledgements

This master thesis was done at the Institute of materials science and engineering at NTNU during the spring 2012.

I wish to thank my supervisors professor Jan Ketil Solberg (NTNU) and Karl Gunnar Solheim (Statoil) for their guidance through this master work.

I would also like to thank Pål Ulseth (NTNU) for his help with sample preparation for TEM and Yingda Yu (NTNU) for his help with TEM.

References

[1] PD Bilmes, M. Solari, and CL Llorente. Characteristics and effects of austenite resulting from tempering of 13cr-nimo martensitic steel weld metals. *Materials characterization*, 46(4):285–296, 2001.

[2] Wayne D. Kaplan David Brandon. *Microstructural Characterization of Materials*. Wiley, 2nd edition, September 2008, page 202-203.

[3] D.Carrouge. 13dissertation, University of Cambridge, 2002.

[4] E.Ladanova. *Microstructural Transformations and Carbide Precipitation in the HAZ of Supermartensitic Stainless Steels*. PhD thesis, NTNU, July 2003.

[5] K.Tsuzaki F.G. Wei. Quantitative analysis on hydrogen trapping of tic particles in steel. *Metallurgical and Materials Transactions A*, 37A(331), February 2006.

[6] E. Folkhard. Welding metallurgy of stainless steels. *E. Folkhard, et. al. 279*, page 6, 1984.

[7] F.Rosenquist. Master thesis 2009. Master thesis, Institute for materials science and engineering, 2009.

[8] AG Haynes. Some factors governing the metallurgy and weldability of 13% cr and newer cr-ni martensitic stainless steels. *Supermartensitic Stainless Steels*, 99(S99-2):25–32, 1999.

[9] R W K Honeycombe. *Steels Microstructure and properties*. Edward Arnold, 41 Bedford Square, London WC1B 3DQ, 1 edition, 1982.

[10] J.K.Solberg. Teknologiske metaller og legeringer. Institutt for materialteknologi, Gløshaugen, Trondheim, August 2010.

[11] J.K.Solberg and V.Hansen. *Innføring i Transmisjon elektronmikroskopi*. NTNU, UiS, 2007.

[12] M. Karlsen, Ø. Grong, M. Søfferud, J. Hjelen, G. Rørvik, and R. Chiron. Scanning electron microscopy/electron backscatter diffraction–based observations of martensite variant selection and slip plane activity in supermartensitic stainless steels during plastic deformation at elevated, ambient, and subzero temperatures. *Metallurgical and Materials Transactions A*, 40(2):310–320, 2009.

[13] K.G.Solheim. *The effect of HAZ Microstructure on the Utilisation Potential of 13Cr Flowlines*. Doctoral thesis, NTNU, January 2012.

[14] M. Kimura, Y. Kitahaba, T. Toyooka, and Y. Miyata. Effect of retained austenite on corrosion performance for modified 13% cr steel pipe. *Corrosion*, 57(05), 2001.

[15] K. Kondo, M. Ueda, K. Ogawa, H. Amaya, H. Hirata, H. Takabe, and Y. Miyazaki. Alloy design of super 13 cr martensitic stainless steel(development of super 13 cr martensitic stainless steel for line pipe-1). *Supermartensitic Stainless Steels'99*, pages 11–18, 1999.

[16] E. Ladanova, JK Solberg, and T. Rogne. Carbide precipitation in haz of multi-pass welds in titanium containing and titanium free supermartensitic stainless steels part 1 proposed precipitation mechanisms. *Corrosion engineering science and technology*, 41(2):143–151, 2006.

[17] P.T. Lovejoy. Structure and constitution of wrought martensitic stainless steels. *Handbook of Stainless Steels, McGraw-Hill, New York*, page 800, 1977.

[18] L.D. Calvert P. Villars. *Pearson's Handbook of Crystallographic Data for Intermetallic Phases, pages 1509-1510,1513,1583*, volume 2. American Society for Metals, Metals Park, Oh 44073, 1985.

[19] A. SmirnovaLasebikan, R. Johnsen, and K. Nisancioglu. Influence of temperature and hydrostatic pressure on hydrogen diffusivity and permeability in 13% cr super martensitic stainless steel under cathodic protection. *CORROSION 2010*, 2010.

[20] J.K. Solberg, E.V.Ladanova, G.Rørvik, and P.E.Kvaale. Post weld heat treatment response of coarse grained heat affected zone in a supermartensitic stainless steel. *Martensitic Stainless Steels'99*, page 56, 1999.

A Appendix

A.1 Hardness, steel A

Table 9: *HV5 readings for steel A after austeniting at* 1000 °C *for 30 minutes. Average and standard deviation is indicated*

Reading no.	**Austenitized [HV5]**
1	367
2	367
3	383
4	365
5	363
6	366
7	368
8	372
9	372
10	368
Average	369
σ	5

Table 10: *HV5 readings for samples of steel A treated at* 500 °C. *Average and standard deviation is indicated*

No.	**Tempering time [min]**													
	1	2	11	12	13	14	15	16	17	18	19	20	30	60
1	354	360	353	377	368	370	366	368	368	367	376	363	362	346
2	345	364	366	363	375	370	359	367	370	366	368	364	363	355
3	352	352	375	375	375	381	356	367	368	364	365	362	361	351
4	362	358	371	366	374	362	376	370	365	370	360	357	363	351
5	355	364	378	377	378	376	358	364	362	365	370	355	359	350
6	355	357	368	360	378	373	365	373	361	366	352	364	360	354
7	351	352	360	366	377	382	364	368	363	363	354	367	368	348
8	361	355	378	378	376	368	367	360	360	364	364	370	360	346
9	352	361	367	368	369	388	377	365	374	371	369	364	369	350
10	351	366	361	365	364	375	377	359	363	363	369	370	367	359
Average	354	359	368	369	373	374	367	366	365	366	365	364	363	351
σ	5	5	8	6	4	7	7	4	4	3	7	5	3	4

Table 11: *HV5 readings for samples of steel A treated at* 550 °C. *Average and standard deviation is indicated*

Reading no.	**Tempering time [min]**													
	1	2	11	12	13	14	15	16	17	18	19	20	30	60
1	357	351	361	370	368	378	374	365	361	351	361	362	361	355
2	352	353	361	365	370	371	362	376	360	357	349	358	363	373
3	360	360	357	381	375	378	379	370	365	359	360	352	358	363
4	354	352	367	383	370	364	376	363	368	368	362	358	363	356
5	354	349	361	382	370	369	380	375	362	372	357	380	360	359
6	351	353	369	377	375	374	368	371	360	372	369	363	359	356
7	359	364	360	368	373	368	356	378	378	370	359	362	358	356
8	357	356	370	372	369	364	370	369	364	368	367	363	361	362
9	346	346	360	378	375	369	366	365	360	357	365	360	354	355
10	342	354	362	373	370	372	367	362	362	360	362	362	359	351
Average	353	354	363	375	372	371	370	369	364	363	361	362	359	358
σ	5	5	4	6	3	5	7	5	5	7	5	7	3	6

Table 12: *HV5 readings for samples of steel A treated at* 600 °C. *Average and standard deviation is indicated*

Reading no.	**Tempering time [min]**													
	1	2	11	12	13	14	15	16	17	18	19	20	30	60
1	348	334	369	352	350	358	350	351	341	348	340	342	341	348
2	333	339	368	360	352	359	348	346	353	332	337	345	339	334
3	344	327	368	352	351	357	350	352	345	337	342	338	331	342
4	338	342	363	366	346	348	354	345	349	342	332	345	337	341
5	342	340	373	360	348	350	342	345	348	338	339	342	341	331
6	331	352	358	354	344	338	343	348	347	347	342	341	339	340
7	335	352	381	367	365	352	358	340	344	348	350	347	340	332
8	336	348	370	370	360	345	353	349	344	336	348	343	343	341
9	341	339	361	372	355	343	349	356	346	338	344	353	339	336
10	354	345	371	353	348	345	355	352	339	347	342	345	341	338
Average	340	342	368	361	352	350	350	348	346	341	341	344	339	338
σ	7	7	6	7	6	7	5	5	4	6	5	4	3	5

A.2 Hardness, steel B

Table 13: *HV5 readings for steel B after austeniting at* 1000 °C *for 30 minutes. Average and standard deviation is indicated*

Reading no.	**Austenitized [HV5]**
1	340
2	332
3	343
4	334
5	330
6	336
7	346
8	349
9	338
10	335
Average	338
σ	6

Table 14: *HV5 readings for samples of steel B treated at* 500 °C. *Average and standard deviation is indicated*

Reading no.	**Tempering time [min]**														
	1	2	10	11	12	13	14	15	16	17	18	19	20	30	60
1	315	301	302	296	299	289	296	307	314	310	313	296	299	287	293
2	310	296	299	297	293	307	307	303	310	317	309	297	293	295	294
3	313	295	298	292	307	287	296	303	309	315	319	306	295	303	293
4	306	305	306	301	298	303	307	305	316	317	305	299	298	301	296
5	306	304	305	301	295	296	307	306	316	318	313	310	303	297	294
6	311	306	306	296	295	302	304	309	318	325	305	312	300	301	298
7	305	301	301	297	291	304	303	303	303	315	316	311	303	304	293
8	308	314	302	295	291	298	302	308	318	322	311	302	304	298	303
9	297	307	295	303	299	302	309	307	313	311	310	291	308	294	292
10	305	317	299	295	305	307	313	305	315	314	313	305	296	298	293
Average	307	305	301	297	297	299	304	306	313	316	311	303	300	298	295
σ	5	7	4	3	5	7	5	2	4	4	4	7	5	5	3

Table 15: *HV5 readings for samples of steel B treated at* 550 °C. *Average and standard deviation is indicated*

Reading no.	**Tempering time [min]**														
	1	2	10	11	12	13	14	15	16	17	18	19	20	30	60
1	282	292	285	295	303	302	308	301	306	311	318	305	308	298	299
2	299	292	291	295	301	308	303	306	317	308	320	313	309	309	299
3	289	301	298	299	299	301	313	315	313	314	313	311	311	305	295
4	292	300	289	299	305	306	306	314	312	315	314	309	310	298	297
5	286	299	295	294	296	305	307	314	315	313	314	311	311	302	305
6	292	307	289	298	307	311	301	312	309	307	318	317	301	304	295
7	292	304	294	299	307	304	306	309	308	317	309	311	309	297	304
8	301	302	296	293	307	308	306	315	312	318	313	313	303	298	301
9	295	310	298	297	300	305	311	315	306	310	314	308	310	302	297
10	291	304	294	292	304	302	305	311	309	312	314	315	303	299	295
Average	292	301	293	296	303	305	306	311	311	312	315	311	307	301	299
σ	5	5	4	2	4	3	3	5	3	3	3	3	4	4	3

Table 16: *HV5 readings for samples of steel B treated at* 600 °C. *Average and standard deviation is indicated*

Reading no.	**Tempering time [min]**														
	1	2	10	11	12	13	14	15	16	17	18	19	20	30	60
1	294	294	309	297	306	306	306	306	309	303	303	308	298	293	294
2	296	309	303	292	300	313	309	313	316	304	305	297	300	298	298
3	299	311	301	306	310	310	309	303	321	308	301	304	299	293	296
4	296	308	308	313	311	308	306	309	318	307	305	308	302	295	291
5	308	299	306	306	309	311	302	312	314	307	302	300	301	293	287
6	297	292	303	312	311	301	302	306	304	304	310	309	298	296	299
7	299	293	304	301	300	300	305	309	319	304	314	301	299	301	289
8	297	296	308	303	312	309	309	312	317	310	311	309	301	296	292
9	292	304	310	305	305	309	311	313	319	306	302	308	304	305	295
10	309	302	306	310	317	302	312	308	308	307	309	309	307	300	288
Average	299	301	306	304	308	307	307	309	314	306	306	305	301	297	293
σ	5	7	3	6	5	4	3	3	5	2	4	4	3	4	4